PERIODIC CRUISE OF A HYPERSONIC CRUISER

FOR FUEL MINIMIZATION

APPROVED: Jason L. Speyer

David B. Hull

PERIODIC CRUISE OF A HYPERSONIC CRUISER FOR FUEL MINIMIZATION

BY

DAVID PAUL DANNEMILLER

THESIS

Presented to the Faculty of the Graduate School of

The University of Texas at Austin

in Partial Fulfillment

of the Requirements

for the Degree of

MASTER OF SCIENCE IN ENGINEERING

THE UNIVERSITY OF TEXAS AT AUSTIN

August 1981

Table of Contents

Section I

Introduction

Without the benefit of definitive investigation, speculation has lead to the assumption that steady state cruise is the most efficient way to cruise an aircraft. Recent work [8,10,11] has shown that this is not the case when trying to minimize average fuel used per distance traveled. Speyer [8] states that a cyclic cruise with large variations from steady state will lead to lower fuel consumption. Walker [11] started an investigation to prove Speyer correct. He found four cycles, all of which were an improvement over steady state, one by as much as 3%. This report will correct, refine, and extend Walker's work.

The purpose of this investigation is to show the complex nature of the optimal periodic cruise problem and to develop numerical techniques to study the problem. Section II describes a four-state hypercruiser model for flight in a vertical plane over a spherical nonrotating earth. A simplification of the spherical earth model leads to a flat earth model. These models are then nondimensionalized and reduced to three-state models to simplify the solution process.

Section III presents a statement of the particular problem to be solved in this investigation. The steady state solutions for the spherical earth and flat earth models developed in Section II are also presented. In Section IV, the general periodic optimal control problem is formulated. The first variation necessary conditions for both the

free final range problem and the fixed final range problem are stated. Section V uses these first variation necessary conditions to develop the hypercruiser as a periodic optimal control problem. Section VI reviews some of the important characteristics of the monodromy matrix. The eigenvalues and eigenvectors of the monodromy matrix are also discussed. Section VII presents the shooting method used in this investigation. Section VIII discusses the algorithms used to trace families of cyclic initial conditions. Section IX discusses the families generated for both the spherical earth and flat earth models. Phase plane plots of a particular cycle are presented to show the character of a cycle. Section X discusses the conclusions that are drawn from this investigation.

Section II

Coordinate System and Model

This Section describes the coordinate system and the model used in this investigation. The nondimensionalization and state reduction of the system are also described.

2.1 Coordinate System

The coordinate system is shown in Figure 1. The x axis is horizontal and positive in the direction of motion. The h axis points away from the center of the earth. The origin of the coordinate system is at sea level directly below the point where the hypercruiser starts its flight.

2.2 Hypercruiser Model

The hypercruiser model chosen for this investigation is a simple one. The reasons for this are two-fold. First, much analytical work has been done on the solution of the flat earth model in the past few years. One of the purposes of this investigation is to verify and quantify this work. The second reason will become more apparent in Section V when the hypercruiser model is formulated as a periodic optimal control problem. During this step, many partial derivatives are taken. A simple model will keep this step tractable.

The differential equations of motion are a simplification of the equations for flight in a vertical plane over a spherical earth. The assumptions contained in the equations are constant gravity, constant

weight, and an isothermal atmosphere, which implies constant speed of sound. The differential equations of motion are

$$\dot{x} = M\, a \cos \gamma \quad , \tag{2.1}$$

$$\dot{h} = M\, a \sin \gamma \quad , \tag{2.2}$$

$$\dot{M} = \frac{g\,(T - D - W \sin \gamma)}{a\, W} \quad , \tag{2.3}$$

$$\dot{\gamma} = \frac{g\,(L - W \cos \gamma)}{M\, a\, W} + \frac{M\, a \cos \gamma}{R_0 + h} \quad , \tag{2.4}$$

where

$\dot{(\ )}$ - d( )/dt ,

x - horizontal distance traveled ,

h - height above sea level ,

M - Mach number ,

γ - flight path angle ,

a - speed of sound, assumed constant ,

g - acceleration due to gravity, assumed constant ;

$g = 32.174 \text{ ft/sec}^2$,

W - weight, assumed constant ; W = 70,000 lb ,

T - thrust ,

D - drag ,

L - lift ,

R_0 - radius of the earth ; $R_0 = 2.1 \times 10^7$ ft .

The assumptions of constant gravity, constant weight, and constant speed of sound are made to simplify the solution process.

The second term in Equation (2.4) is the contribution to the equations of motion due to the spherical earth. Several times throughout this report, reference will be made to the flat earth solution. This solution is obtained using Equations (2.1) through (2.4) without the spherical earth term.

The temperature and pressure models are from the stratospheric layer of the standard atmosphere. Temperature is assumed constant, $\Theta = 390\ ^{o}R$, where Θ denotes absolute temperature. The pressure model is

$$p = C_1 e^{C_2 h} \quad , \tag{2.5}$$

where C_1 and C_2 are constants whose values are

$$C_1 = 2.6783378 \times 10^{3}\ lb/ft^2 \quad ,$$

$$C_2 = -4.8100264 \times 10^{-5}\ 1/ft \quad .$$

The assumption of constant temperature leads to constant speed of sound, $a = 967.705$ ft/sec .

The models for lift and drag are

$$L = \frac{1}{2} p k M^2 b^2 C_L \quad , \tag{2.6}$$

$$D = \frac{1}{2} p k M^2 b^2 C_D \quad , \tag{2.7}$$

$$C_D = C_{D_0} + K C_L^2 \quad , \tag{2.8}$$

where

k - ratio of specific heats ; $k = 1.4$,

b^2 - reference area ; $b^2 = 576\ ft^2$,

C_L - coefficient of lift ,

C_D - coefficient of drag ,

C_{D_0} - coefficient of zero-lift drag ; $C_{D_0} = .02$,

K - coefficient of induced drag ; $K = .8$.

The assumption of constant aerodynamic coefficients C_{D_0} and K is good in the higher Mach number region but may be questionable at lower Mach numbers. Later, solutions of interest will be shown in the Mach 2 region. These solutions can be used to show trends but should be used carefully when quantifing those trends.

Thrust and coefficient of lift are selected as controls. They may be varied as desired within bounds. No bounds are put on the coefficient of lift. When an interesting solution is found, the C_L history should be checked to make sure it is reasonable. The bounds on thrust are

$$0 \leq T \leq T_{max} \quad , \tag{2.9}$$

where maximum thrust is $T_{max} = 50{,}000$ lb.

The model for fuel flow is

$$\dot{w}_f = \sigma T \quad , \tag{2.10}$$

$$\sigma = \text{/} M \quad , \tag{2.11}$$

where

w_f - weight of fuel consumed ,

σ - thrust specific fuel consumption ,

ℓ - constant ; ℓ = .1 1/sec .

The constant ℓ is chosen for convenience. Because of this, the amount of fuel used which is generated by this model should not be viewed as an absolute number but as a performance measure to compare different control strategies.

The models for T_{max} and σ are the most limiting assumptions. Both T_{max} and σ should vary with h and M. In this study, T_{max} is constant and σ is linear with M. As mentioned earlier, these assumptions are made to allow the algebra in Section V to remain tractable.

When the periodic cruise problem is studied, it is assumed that the engine can be turned on and off instantaneously. At first, this may sound like a bad assumption, but the engine used for this study is a SCRAM (Supersonic Combustion RAMjet) engine. It is similar to a ramjet engine in that it has no turbines. Since there are no turbines, there is no spool-up time. To start the engine, inject fuel into the engine and ignite it. To stop the engine, shut off the flow of fuel. Both of these operations can be done very quickly, so the assumption that they occur instantaneously is not bad.

2.3 Nondimensionalization and Reduction of State

To improve the precision of integration, Equations (2.1) and (2.2) are nondimensionalized by the constant F. The resulting set of equations is

$$\dot{\bar{x}} = \frac{M\ a \cos \gamma}{F} \quad , \tag{2.12}$$

$$\dot{\bar{h}} = \frac{M\ a \sin \gamma}{F} \quad , \tag{2.13}$$

$$\dot{M} = \frac{g\ (T - D - W \sin \gamma)}{a\ W} \quad , \tag{2.14}$$

$$\dot{\gamma} = \frac{g\ (L - W \cos \gamma)}{M\ a\ W} + \frac{M\ a \cos \gamma}{(R_0 + h)} \quad , \tag{2.15}$$

where

$\bar{x}$ - nondimensional range ; $\bar{x} = x/F$,

$\bar{h}$ - nondimensional altitude ; $\bar{h} = h/F$,

F - nondimensionalization factor ; F = 500,000 ft .

Equations (2.12) through (2.15) represent a four-dimensional system. Since time does not appear explicitly in the equations, this four-dimensional system can be reduced to a three-dimensional system by dividing Equations (2.13) through (2.15) by Equation (2.12) . This causes nondimensional range $\bar{x}$ to become the independent variable. For equation (2.13), this division is

$$(\dot{\bar{h}}/\dot{\bar{x}}) = (d\bar{h}/dt)/(d\bar{x}/dt) = (d\bar{h}/d\bar{x}) = \bar{h}' \quad ,$$

where $(\ )'$ denotes $d(\ )/d\bar{x}$. The new three-dimensional system is

Section III

Problem Statement and Steady State Solution

This Section presents the problem statement of the optimal control problem and the steady state solution for both the flat earth and the spherical earth models.

3.1 Problem Statement

Minimize with respect to the control functions $[C_L(\bar{x}), T(\bar{x})]$, the period $\bar{x}_f$, and the initial conditions $[\bar{h}(0), M(0), \gamma(0)]$

$$J = \frac{1}{\bar{x}_f} \int_0^{\bar{x}_f} \frac{T}{a \cos \gamma} \, d\bar{x} \quad , \tag{3.1}$$

subject to the differential constraints

$$\bar{h}' = \tan \gamma \quad , \tag{3.2}$$

$$M' = \frac{g F (T - D - W \sin \gamma)}{M a^2 W \cos \gamma} \quad , \tag{3.3}$$

$$\gamma' = \frac{g F (L - W \cos \gamma)}{M^2 a^2 W \cos \gamma} + \frac{1}{\bar{R}_0 + \bar{h}} \quad , \tag{3.4}$$

the boundary conditions

$$\bar{h}(0) = \bar{h}(\bar{x}_f) \quad , \tag{3.5}$$

$$M(0) = M(\bar{x}_f) \quad , \tag{3.6}$$

$$\gamma(0) = \gamma(\bar{x}_f) \quad , \tag{3.7}$$

and the control inequality constraint

$$0 \leq T \leq T_{max} \quad . \tag{3.8}$$

3.2 Steady State Solution

During steady state flight, $\gamma = 0$ and $T = D$, so the integrand of the performance index J is constant, thus, Equation (3.1) becomes

$$J_{ss} = \frac{\ell D}{a} \tag{3.9}$$

where J_{ss} denotes steady state performance index.

Since ℓ and a are constant, minimizing Equation (3.9) implies minimizing D. In order to get an expression for D, an expression for L is needed. To get an expression for L, Equation (2.4) is used. Recall that for steady state flight $\gamma=0$ and $\dot{\gamma}=0$. Make these substitutions into Equation (2.4) and solve for L :

$$L_{ss} = W - \frac{M^2 a^2 W}{g (R_0 + h)} \quad , \tag{3.10}$$

where L_{ss} denotes steady state lift.

One way to eliminate the spherical earth term is to let $R_0 \rightarrow \infty$. When this is done, the second term in Equation (3.10) vanishes. This gives the proper lift for steady state cruise over a flat earth, L = W.

Equation (3.10) combined with

$$q = \frac{1}{2} p k M^2 b^2 \quad , \tag{3.11}$$

$$L = q C_L \quad , \tag{3.12}$$

$$D = q (C_{D_0} + K C_L^2) \quad , \tag{3.13}$$

gives the steady state drag

$$D_{ss} = q C_{D_0} + \frac{K W^2}{q} (1 - \frac{M^2 a^2}{g (R_0 + h)})^2 \quad , \tag{3.14}$$

where q denotes dynamic pressure and D_{ss} denotes steady state drag .

Equation (3.14) is minimized using a numerical one-dimensional search technique. Mach number is specified and a search is conducted for the altitude which produces minimum drag for that Mach number. The results are shown in Figures 2a and 2b. Figure 2a shows altitude vs. Mach number for the best steady state cruise over a spherical earth. Figure 2b is for steady state cruise over a flat earth. Note that Figure 2b is a curve of constant dynamic pressure corresponding to flight at maximum lift over drag.

Steady state performance vs. Mach number for cruise over a spherical earth is shown in Figure 2c. Figure 2d is for steady state cruise over a flat earth. Note the performance index for the flat earth case is constant. For the spherical earth case, the improvement in the performance index at increasing Mach number is due solely to the spherical earth term.

Section IV

Derivation of the Periodic Optimal Control Problem

In this section, the first variation necessary conditions for the free final range and the fixed final range problems are derived.

Section III describes the specific problem to be solved in this investigation. Before deriving the optimal control problem, a more general problem will be stated. Minimize

$$J = \frac{1}{\bar{x}_f} \int_0^{\bar{x}_f} L(X,U)\, d\bar{x} \quad , \tag{4.1}$$

subject to the differential constraints

$$X' = f(X,U) \quad , \tag{4.2}$$

the prescribed boundary conditions

$$\Psi(X(0),X(\bar{x}_f)) = 0 \quad , \tag{4.3}$$

and the control inequality constraint

$$U_{min} \leq U \leq U_{max} \quad . \tag{4.4}$$

where

X - state vector,

U - control vector,

f - set of differential equations.

Form the augmented performance index :

$$J' = \mu^T \Psi + \frac{1}{\bar{x}_f} \int_0^{\bar{x}_f} [\, L + \lambda^T f - \lambda^T X' \,]\, d\bar{x} \quad . \tag{4.5}$$

Here μ and λ are vectors of Lagrange multipliers and the prime on J' is used to distinguish it from J. Define

$$G = \mu^T \Psi \quad , \tag{4.6}$$

$$H = L + \lambda^T f \quad . \tag{4.7}$$

Substitute Equations (4.6) and (4.7) into Equation (4.5). The augmented performance index becomes

$$J' = G + \frac{1}{\bar{x}_f} \int_0^{\bar{x}_f} [\, H - \lambda^T X' \,]\, d\bar{x} \quad . \tag{4.8}$$

The first variation of J' is

$$\delta J' = G_{X_0}\, \delta X_0 + G_{X_f}\, \delta X_f - \frac{\delta \bar{x}_f}{\bar{x}_f{}^2} \int_0^{\bar{x}_f} [\, H - \lambda^T X' \,]\, d\bar{x}$$

$$+ \frac{1}{\bar{x}_f} [(H - \lambda^T X')\delta \bar{x}]_0^{\bar{x}_{c-}} + \frac{1}{\bar{x}_f} \int_0^{\bar{x}_{c-}} [H_X \tilde{\delta} X + H_U \tilde{\delta} U - \lambda^T \tilde{\delta} X']\, d\bar{x}$$

$$+\frac{1}{\bar{x}_f}\Big[\quad''\quad\Big]_{\bar{x}_{c+}}^{\bar{x}_f}+\frac{1}{\bar{x}_f}\int_{\bar{x}_{c+}}^{\bar{x}_f}\Big[\quad''\quad\Big]d\bar{x}\,, \tag{4.9}$$

where

$\tilde{\delta}(\ )$ - variation of ( ) holding $\bar{x}$ constant,

$\delta(\ )$ - total variation of ( ).

The limits of integration are broken at $\bar{x}_c$ because the derivative of the integral is discontinuous at that point. The point physically corresponds to the point where the control is discontinuous. For simplicity only one discontinuous point is assumed here. Note that

$$\frac{1}{\bar{x}_f}\int_0^{\bar{x}_f}[\,H-\lambda^T X'\,]\,d\bar{x}=J\,, \tag{4.10}$$

$$\int_a^b \lambda^T\,\tilde{\delta}X'\,d\bar{x}=\lambda^T\,\tilde{\delta}X\Big]_a^b-\int_a^b \lambda'^T\,\tilde{\delta}X\,d\bar{x}\,, \tag{4.11}$$

$$\tilde{\delta}X=\delta X-X'\,\delta\bar{x}\,, \tag{4.12}$$

$$\delta\bar{x}_0=0\,, \tag{4.13}$$

$$\delta\bar{x}_{c+}=\delta\bar{x}_{c-}=\delta\bar{x}_c\,, \tag{4.14}$$

$$\delta X_{c+}=\delta X_{c-}=\delta X_c\,, \tag{4.15}$$

$$\underline{\Delta}(\ )=(\ )_{c+}-(\ )_{c-}\,. \tag{4.16}$$

Substitute Equations (4.10) through (4.16) into Equation (4.9) and collect terms. The first variation becomes

$$\delta J' = \left(G_{X_0} + \frac{\lambda^T{}_0}{\bar{x}_f} \right) \delta X_0 + \left(\frac{1}{\bar{x}_f} \Delta \lambda^T \right) \delta X_c + \left(\frac{1}{\bar{x}_f} \Delta H \right) \delta \bar{x}_c$$

$$+ \left(G_{X_f} - \frac{\lambda^T{}_f}{\bar{x}_f} \right) \delta X_f + \left(- \frac{J}{\bar{x}_f} + \frac{H_f}{\bar{x}_f} \right) \delta \bar{x}_f$$

$$+ \frac{1}{\bar{x}_f} \int_0^{\bar{x}_{c-}} \left[\left(H_X + \lambda'^T \right) \delta X + H_U \, \delta U \right] d\bar{x}$$

$$+ \frac{1}{\bar{x}_f} \int_{\bar{x}_{c+}}^{\bar{x}_f} [\quad " \quad] \, d\bar{x} \quad . \qquad (4.17)$$

In order for the first variation to vanish, a necessary condition for a minimum, the following conditions must be satisfied :

Differential Constraints

$$X' = f \quad , \qquad (4.18)$$

Euler Equations

$$H_X + \lambda'^T = 0 \quad , \qquad (4.19)$$

$$H_U \, \delta U = 0 \quad , \qquad (4.20)$$

Prescribed Boundary Conditions

$$\Psi = 0 \quad , \tag{4.21}$$

Natural Boundary Conditions

$$G_{X_0} + \frac{\lambda_0^T}{\bar{x}_f} = 0 \quad , \tag{4.22}$$

$$G_{X_f} - \frac{\lambda_f^T}{\bar{x}_f} = 0 \quad , \tag{4.23}$$

$$-J + H_f = 0 \quad , \tag{4.24}$$

Natural Corner Conditions

$$\underset{\sim}{\wedge} \lambda = 0 \quad , \tag{4.25}$$

$$\underset{\sim}{\wedge} H = 0 \quad . \tag{4.26}$$

The Hamiltonian, as defined in Equation (4.7), is a function of X, U, and λ. Since it is not a function of the independent variable $\bar{x}$, the Hamiltonian is constant during the cycle.

Equation (4.20) is slightly different from the other conditions. The difference is caused by Equation (4.4) which is the control inequality constraint. Equation (4.20) is satisfied in one of two ways. If $H_U = 0$, the control takes on a value which is in the interior of the inequality constraint of Equation (4.4). If the control tends to take a value outside the inequality constraint, Equation (4.20) is satisfied by setting the control on the boundary and setting $\underset{\sim}{\delta} U = 0$.

The above conditions are the first variation necessary conditions for the free final range problem. This is the problem in which the final range after one cycle is not specified. For the fixed final range problem, the conditions are the same except for one. Equation (4.24) comes from the $\delta\overline{x}_f$ term in Equation (4.17). In the fixed final range problem, the final range is specified so $\delta\overline{x}_f = 0$. Therefore, Equation (4.24) is not present in the fixed final range problem.

Section V

Hypercruiser as an Optimal Control Problem

This Section uses the results of Section IV to formulate the hypercruiser as an optimal control problem.

5.1 Hamiltonian

Form the Hamiltonian

$$H = L + \lambda^T f \quad ,$$

$$= \frac{\ell T}{a \cos \gamma} + \lambda_{\bar{h}} \bar{h}' + \lambda_M M' + \lambda_\gamma \gamma' \quad ,$$

$$= \frac{\ell T}{a \cos \gamma} + \lambda_{\bar{h}} \tan \gamma + \lambda_M \frac{g F (T - D - W \sin \gamma)}{M a^2 W \cos \gamma} \quad ,$$

$$+ \lambda_\gamma \frac{g F (L - W \cos \gamma)}{M^2 a^2 W \cos \gamma} + \lambda_\gamma \frac{1}{\bar{R}_0 + \bar{h}} \quad . \tag{5.1}$$

The $\bar{h}$ subscript on $\lambda_{\bar{h}}$ denotes that $\lambda_{\bar{h}}$ is the component of the λ vector associated with the $\bar{h}'$ differential equation. Similar notation is used for the other λ's. Since the Hamiltonian is not a function of the independent variable $\bar{x}$, it is a constant of the motion. This is useful to use as a check when numerical routines are tested.

5.2 Controls

Equation (4.20) is used to derive the equations for the controls C_L and T. The equation for C_L will be derived first. Since there are no bounds on C_L and since C_L is not singular, Equation (4.20) is satis-

fied by $H_{C_L} = 0$:

$$H_{C_L} = 0 = -\lambda_M \frac{g\ F\ D_{C_L}}{M\ a^2\ W \cos \gamma} + \lambda_\gamma \frac{g\ F\ L_{C_L}}{M^2\ a^2\ W \cos \gamma} \quad , \tag{5.2}$$

where

$$D_{C_L} = p\ k\ M^2\ b^2\ K\ C_L \quad , \tag{5.3}$$

$$L_{C_L} = \frac{1}{2}\ p\ k\ M^2\ b^2 \quad , \tag{5.4}$$

Substitute Equations (5.3) and (5.4) into Equation (5.2), and solve for C_L. The result is the equation for the C_L control,

$$C_L = \frac{\lambda_\gamma}{2\ \lambda_M\ M\ K} \quad . \tag{5.5}$$

The thrust equation is not quite so straightforward. Since $H_{TT} \equiv 0$, the thrust control is singular. The thrust control is obtained by using Pontryagin's "Minimum Principle" on Equation (4.20) :

$$T = \begin{cases} T_{max} & ; H_T < 0 \\ 0 & ; H_T > 0 \end{cases} \quad , \tag{5.6}$$

$$H_T = \frac{\lambda_V}{a \cos \gamma} + \lambda_M \frac{g\ F}{M\ a^2\ W \cos \gamma} \quad . \tag{5.7}$$

H_T is known as a switching function because when $H_T = 0$, the thrust is switched from on to off or vice versa. This form of the control only allows maximum thrust or no thrust. If $H_T = 0$ for a finite interval of time allowing intermediate values of thrust (a singular arc in the

calculus of variations [3]), a chattering of thrust would occur. This phenomenon has not been observed by the author.

5.3 λ Differential Equations

The differential equations for λ are obtained from Equation (4.19). Equation (5.5) is used to do some simplification :

$$\lambda_{\bar{h}}' = -H_{\bar{h}} = \frac{\lambda_M g F^2 C_2 D}{M a^2 W \cos \gamma} - \frac{\lambda_\gamma g F^2 C_2 L}{M^2 a^2 W \cos \gamma} + \frac{\lambda_\gamma}{(\bar{R}_0 + \bar{h})^2} \quad , \tag{5.8}$$

$$\lambda_M' = -H_M = \frac{\lambda_M g F (T - D - W \sin \gamma)}{M^2 a^2 W \cos \gamma} + \frac{\lambda_M g F p k b^2 C_{D_0}}{a^2 W \cos \gamma} + \frac{2 \lambda_\gamma g F (L - W \cos \gamma)}{M^3 a^2 W \cos \gamma} - \frac{\lambda_\gamma^2 g F p k b^2}{4 \lambda_M M^2 a^2 W K \cos \gamma} \quad , \tag{5.9}$$

$$\lambda_\gamma' = -H_\gamma = -\frac{(/ T \sin \gamma}{a \cos^2 \gamma} - \frac{\lambda_{\bar{h}}}{\cos^2 \gamma} - \frac{\lambda_M g F \sin \gamma (T - D)}{M a^2 W \cos^2 \gamma} + \frac{\lambda_M g F}{M a^2 \cos^2 \gamma} - \frac{\lambda_\gamma g F L \sin \gamma}{M^2 a^2 W \cos^2 \gamma} \quad . \tag{5.10}$$

5.4 Boundary Conditions

The prescribed boundary conditions state that

$$\Psi = X(\bar{x}_f) - X(0) = 0 \quad ,$$

$$X(\bar{x}_f) = X(0) \quad , \tag{5.11}$$

where $X = [\ \bar{h}\ ,\ M\ ,\ \gamma\ ]^T$. This means the initial altitude must equal the final altitude, the initial Mach number must equal the final Mach number, and the initial flight path angle must equal the final flight path angle. Equations (4.22) and (4.23) will be used to show that λ must be periodic. G is defined as

$$G = \mu^T \Psi = \mu^T (X(\bar{x}_f) - X(0)) \quad . \tag{5.12}$$

Take the partial derivatives of G, substitute them into Equations (4.22) and (4.23), and add (4.22) and (4.23). The resulting equation is

$$-\mu^T + \frac{\lambda^T 0}{\bar{x}_f} + \mu^T - \frac{\lambda^T f}{\bar{x}_f} = 0 \quad . \tag{5.13}$$

This gives the result

$$\lambda(0) = \lambda(\bar{x}_f) \quad . \tag{5.14}$$

Thus, not only is X required to be periodic, but Equations (4.22) and (4.23) require λ to be periodic. Since H is a constant of the motion, Equation (4.24) becomes H = J.

5.5 New State Vector

Combine the X and λ vectors to form a new state vector Z where

$$Z = \begin{bmatrix} X \\ \lambda \end{bmatrix} \quad . \tag{5.15}$$

The differential equation for this new state vector is

$$Z' = \begin{bmatrix} X' \\ \lambda' \end{bmatrix} = \bar{f}(Z) \quad . \tag{5.16}$$

The Euler equations have been used to eliminate the control from the differential equations. The range derivative of the state vector Z is a function only of itself. This means that given an initial value for the state vector, Z(0), and the final range, $\bar{x}_f$, the state at the final range, $Z(\bar{x}_f)$, is uniquely determined. Further, through the use of Equations (4.21) through (4.23), the very compact requirement $Z(0) = Z(\bar{x}_f)$ is obtained.

5.6 Corner Conditions

A corner occurs when the thrust is turned on or off. This causes a discontinuity in the derivative of the state vector Z. Equation (4.15) implies that the vector X must be continuous at a corner point. Equation (4.25) states that the Lagrange multipliers λ must be continuous at a corner. These two imply $\Delta Z = 0$.

Equation (4.26) states that the Hamiltonian must remain constant when the thrust is changed. This condition is automatically satisfied because the thrust changes when $H_T = 0$.

5.7 Transition Matrix

Methods to be developed later in this report make use of the transition matrix of the cycle. The transition matrix is a linearization about the path and can be used to map initial variations to final

variations.

$$\delta Z_f = \Phi(\bar{x}_f,0)\ \delta Z_0 \quad , \tag{5.17}$$

where $\Phi(\bar{x}_f,0)$ denotes the transition matrix from initial range to final range. The transition matrix differential equation is

$$\Phi'(\bar{x},0) = A(\bar{x})\ \Phi(\bar{x},0) \quad ; \ \Phi(0,0) = I \quad , \tag{5.18}$$

$$A = \frac{\partial \bar{f}}{\partial Z} \quad , \tag{5.19}$$

$$\bar{f} = Z' \quad . \tag{5.20}$$

The A matrix is 6 by 6. It's elements are listed in Appendix A for convenience. The differential equation for Φ assumes continuous δ variations. This condition is satisfied everywhere on the path except where the engine turns on or off. These corner points cause discontinuities in the δ variations which cause jumps in Φ. Following is the derivation of the transfer matrix $\Phi(\bar{x}_{c+},\bar{x}_{c-})$ which causes jumps in the transition matrix. Refer to Figure 3 for the notation used in the derivation.

The variation of Z at $\bar{x}_{c-}$ can be calculated using the transition matrix $\Phi(\bar{x}_{c-},0)$

$$\delta Z_{c-} = \Phi(\bar{x}_{c-},0)\ \delta Z_0 \quad . \tag{5.21}$$

The variation δZ_{c-} causes the corner to occur at $\bar{x}_{c+}$. The change in the location of the corner, $\delta\bar{x}_c$, is calculated as follows :

$$H_T(Z) = 0 \quad , \tag{5.22}$$

$$\delta H_T = 0 = H_{TZ}\delta Z \quad , \tag{5.23}$$

$$= H_{TZ_{c-}} [\tilde{\delta} Z_{c-} + Z'_{c-} \bar{\delta x}_c] \quad , \tag{5.24}$$

$$0 = H_{TZ_{c-}} \tilde{\delta} Z_{c-} + H_{TZ_{c-}} Z'_{c-} \bar{\delta x}_c \quad , \tag{5.25}$$

$$\bar{\delta x}_c = - \frac{H_{TZ_{c-}} \tilde{\delta} Z_{c-}}{H_{TZ_{c-}} Z'_{c-}} \quad . \tag{5.26}$$

The relationship between $\tilde{\delta} Z_{c-}$ and $\tilde{\delta} Z_{c+}$ is calculated as follows :

$$\delta Z_c = \tilde{\delta} Z_{c-} + Z'_{c-} \bar{\delta x}_c = \tilde{\delta} Z_{c+} + Z'_{c+} \bar{\delta x}_c \quad , \tag{5.27}$$

$$\tilde{\delta} Z_{c+} = \tilde{\delta} Z_{c-} - [Z'_{c+} - Z'_{c-}] \bar{\delta x}_c \quad . \tag{5.28}$$

Combine Equations (5.26) and (5.28) to give

$$\tilde{\delta} Z_{c+} = \tilde{\delta} Z_{c-} + [Z'_{c+} - Z'_{c-}] \frac{H_{TZ_{c-}} \tilde{\delta} Z_{c-}}{H_{TZ_{c-}} Z'_{c-}} \quad , \tag{5.29}$$

$$= \{ I + [Z'_{c+} - Z'_{c-}] \frac{H_{TZ_{c-}}}{H_{TZ_{c-}} Z'_{c-}} \} \tilde{\delta} Z_{c-} \quad . \tag{5.30}$$

The term in the braces of Equation (5.30) is the transition matrix from $\bar{x}_{c-}$ to $\bar{x}_{c+}$. Use the properties of transition matrices to give

$$\Phi(\bar{x}_{c+}, 0) = \Phi(\bar{x}_{c+}, \bar{x}_{c-}) \Phi(\bar{x}_{c-}, 0) \quad , \tag{5.31}$$

$$\Phi(\bar{x}_{c+},\bar{x}_{c-}) = \{ I + [Z'_{c+} - Z'_{c-}] \frac{H_{TZ_{c-}}}{H_{TZ_{c-}} Z'_{c-}} \} \quad . \qquad (5.32)$$

The algorithm for calculating the final state, transition matrix, and fuel used is summarized below.

1) Initialize :

   $Z(0)$ - guess,

   $\bar{x}_f$ - guess,

   $\Phi(0,0) = I$,

   $w_f = 0$.

2) Integrate one step.

3) If final range is reached, go to 6.

4) If no thrust change, go to 2.

5) Thrust change :

   find thrust change point very accurately using $H_T = 0$,

   change thrust,

   calculate $\Phi(\bar{x}_{c+},\bar{x}_{c-})$,

   calculate $\Phi(\bar{x}_{c+},0) = \Phi(\bar{x}_{c+},\bar{x}_{c-})\ \Phi(\bar{x}_{c-},0)$,

   go to 2.

6) Final range reached :

   calculate $J = \frac{w_f}{\bar{x}_f}$,

   stop.

The state has 6 differential equations, the transition matrix has 36 differential equations, and the equation for fuel used is 1

differential equation. This is a total of 43 equations which must be integrated.

Section VI

Monodromy Matrix, Eigenvalues, and Eigenvectors

This Section starts off with a review of some of the important characteristics of the monodromy matrix. Stability coefficients are then presented to simplify the presentation of eigenvalues. Finally, a method for computing eigenvectors is presented.

6.1 Properties of Monodromy Matrix

The monodromy matrix is the transition matrix evaluated over one cycle. [5] and [9] describe many of the properties of the monodromy matrix in detail. Some of the important properties are repeated here.

The monodromy matrix is symplectic which means it satisfies

$$\mathbf{\Phi}\, K\, \mathbf{\Phi}^T = K \quad , \tag{6.1}$$

where

$$K = \begin{bmatrix} 0 & I \\ -I & 0 \end{bmatrix} \quad .$$

Identity (6.1) is a useful check on the numerical accuracy of the monodromy matrix. Another useful property of a symplectic matrix is the occurance of eigenvalues in reciprocal pairs; that is, if one eigenvalue is λ_i, i=1,2,3, another eigenvalue is $\lambda_{i+3} = 1/\lambda_i$, i=1,2,3. Since the monodromy matrix is real valued, imaginary eigenvalues occur in complex conjugate pairs.

Another important fact is the monodromy matrix always contains two unity eigenvalues. The two unity eigenvalues are coupled so they form a Jordan box. The Jordan form of $\mathbf{\Phi}$ is

$$\begin{bmatrix} \lambda_1 & & & & & \\ & \frac{1}{\lambda_1} & & & & \\ & & \lambda_2 & & & \\ & & & \frac{1}{\lambda_2} & & \\ & & & & 1 & 1 \\ & & & & & 1 \end{bmatrix} \tag{6.2}$$

When all the above facts are combined, it can be seen that the allowable eigenvalue patterns of the monodromy matrix are severely restricted. Figure 4 shows all possible combinations of the eigenvalues.

The primary eigenvector associated with one of the unity eigenvalues is the initial derivative vector $Z'(0)$, i.e. $(\mathbf{\Phi}-I)Z'(0) = 0$. If the initial conditions of a cycle are perturbed so that a new cycle occurs, a family of cycles results. That is,

$$\delta Z(\bar{x}_f) = \delta Z(0) \quad ,$$

$$\tilde{\delta} Z(\bar{x}_f) + Z'(\bar{x}_f)\delta\bar{x}_f = \mathbf{\Phi}\tilde{\delta} Z(0) + Z'(0)\delta\bar{x}_f = \tilde{\delta} Z(0) \quad , \tag{6.3}$$

$$(\mathbf{\Phi}-I)\tilde{\delta} Z(0) = -Z'(0)\delta\bar{x}_f \quad . \tag{6.4}$$

Equation (6.4) shows that the second-order generalized eigenvector associated with the other unity eigenvalue is the family direction.

6.2 Stability Coefficients

In [2], Broucke describes two real valued scalars a_1 and a_2 called stability coefficients. These stability coefficients are used to simplify the presentation of eigenvalues. Since Broucke's problem is two-dimensional, his stability coefficients are the coefficients of the characteristic equation of the monodromy matrix. The hypercruiser problem is three-dimensional. The stability coefficients are still coefficients of the characteristic equation, but the characteristic equation is in the form

$$(s - 1)^2 (s^4 + a_1 s^3 + a_2 s^2 + a_1 s + 1) = 0 \quad . \tag{6.5}$$

The coefficients a_1 and a_2 are related to the eigenvalues of the monodromy matrix as

$$a_1 = - (\lambda_1 + \frac{1}{\lambda_1} + \lambda_2 + \frac{1}{\lambda_2}) \quad , \tag{6.6}$$

$$a_2 = (\lambda_1 + \frac{1}{\lambda_1}) (\lambda_2 + \frac{1}{\lambda_2}) + 2 \quad , \tag{6.7}$$

but, a_1 and a_2 can be calculated without first calculating the eigenvalues. This is done as follows :

$$S_1 = \mathrm{Tr}(\mathbf{B}) \quad , \tag{6.8}$$

$$S_2 = \mathrm{Tr}(\mathbf{B}\,\mathbf{B}) \quad , \tag{6.9}$$

$$a_1 = -S_1 + 2 \quad , \tag{6.10}$$

$$a_2 = -\frac{1}{2}(S_2 - S_1^2) - 2 S_1 + 3 \quad , \tag{6.11}$$

where Tr( ) indicates the trace of ( ). The a_1, a_2 plane is divided into 7 regions as shown in Figure 5. The regions are separated by the two straight lines,

$$a_2 = 2\,a_1 - 2 \tag{6.12}$$

which corresponds to $\lambda_i = \lambda_{i+3} = -1$,

$$a_2 = -2\,a_1 - 2 \tag{6.13}$$

which corresponds to $\lambda_i = \lambda_{i+3} = 1$, and the parabola

$$a_2 = \frac{1}{4}\,a_1^2 + 2 \tag{6.14}$$

which corresponds to $\lambda_i = \lambda_{i+1}$ and $\lambda_{i+3} = \lambda_{i+4} = \frac{1}{\lambda_i}$.

The form of the eigenvalues for each region is also shown in Figure 4 . Everytime a_1, a_2 crosses a line described by Equations (6.12) through (6.14), an interesting event happens. For instance, when a_1, a_2 go from region 6 to region 1, the distinct eigenvalues on the real axis coalesce at unity and then break off the real axis onto the unit circle. Other events can easily be identified by studying Figure 5. The introduction of a_1 and a_2 greatly simplifies the presentation of the eigenvalues of the family.

6.3 Calculating Eigenvectors

There are three problems with using a general purpose eigenvector routine in this investigation. First, the unity eigenvalues are usually unity only to about 5 decimal places. Because of this accuracy

problem, a general purpose eigenvector routine treats the two unity eigenvalues as distinct. Instead of returning a primary eigenvector and a second order generalized eigenvector for the two unity eigenvalues, two primary eigenvectors are returned which are very close to being linearly related.

The second problem is the errors in the unity eigenvalues may be in the form of small imaginary parts on the order of 10^{-5}. These small imaginary parts sometimes cause large imaginary components in the eigenvectors. The primary eigenvector should be equal to the initial derivative vector of the system. It makes no physical sense for this problem to have an imaginary part in the initial derivative vector.

The third problem is that eigenvectors are not unique. By allowing a general purpose eigenvector routine to calculate eigenvectors, it is not possible to take full advantage of the non-uniqueness of eigenvectors. This non-uniqueness is especially useful when calculating the second order generalized eigenvectors associated with the unity eigenvalue of $\mathbf{0}$.

The calculation of eigenvectors involves the solution of a linear system of the form

$$A\,x = y \quad , \tag{6.15}$$

where A is a 2n by 2n matrix of rank m where $m < 2n$. The solution of Equation (6.15) is obtained by first partitioning the linear system :

$$\begin{bmatrix} A_{11} & A_{12} \\ A_{21} & A_{22} \end{bmatrix} \begin{bmatrix} x_1 \\ x_2 \end{bmatrix} = \begin{bmatrix} y_1 \\ y_2 \end{bmatrix} \quad , \tag{6.16}$$

where A_{11} is m by m and full rank, and all other sub-matrices are conformable. Since A is rank m, the identity

$$A_{22} - A_{21}A_{11}^{-1}A_{12} = 0 \tag{6.17}$$

is satisfied. Further, in order for a solution of Equation (6.16) to exist, the linear system represented by A and y must be consistent [1]; that is, it must satisfy the identity

$$y_2 - A_{21}A_{11}^{-1}y_1 = 0 \quad . \tag{6.18}$$

If this condition is satisfied, the solution to (6.16) is

$$x = \begin{bmatrix} x_1 \\ x_2 \end{bmatrix} = \begin{bmatrix} A_{11}^{-1} y_1 \\ 0 \end{bmatrix} + \begin{bmatrix} - A_{11}^{-1} A_{12} \\ I \end{bmatrix} x_2 \quad , \tag{6.19}$$

where x_2 is an arbitrary (2n-m) vector.

The primary and second order generalized eigenvectors associated with the two coupled unity eigenvalues must satisfy

$$A\,p = 0 \quad , \tag{6.20}$$

$$A\,s = p \quad , \tag{6.21}$$

where $A = (\beta - I)$, p is the primary eigenvector, and s is the second order generalized eigenvector. Apply Equation (6.19) to the solution of Equations (6.20) and (6.21) to give

$$p = \begin{bmatrix} p_1 \\ p_2 \end{bmatrix} = \begin{bmatrix} -A_{11}^{-1} A_{12} \\ I \end{bmatrix} p_2 \quad , \tag{6.22}$$

$$s = \begin{bmatrix} s_1 \\ s_2 \end{bmatrix} = \begin{bmatrix} -A_{11}^{-1} A_{11}^{-1} A_{12} \\ 0 \end{bmatrix} p_2 + \begin{bmatrix} -A_{11}^{-1} A_{12} \\ I \end{bmatrix} s_2 \quad . \tag{6.23}$$

From Equation (6.2), it is seen that A is 6 by 6 of rank 5. Thus, in Equations (6.22) and (6.23), all terms in brackets are 6 by 1, and p_2 and s_2 are scalars.

Section VII

Shooting Method

This Section describes the shooting method used in this investigation. Following the derivation of the shooting method is a discussion of its performance.

7.1 Derivation of Shooting Method

A shooting method is an algorithm applied iteratively to a system. The object of each iteration is to adjust a set of parameters in a manner that will drive a set of conditions to zero. When the conditions are zero, the method is said to have converged. The solution to which the shooting method converges must be unique in the immediate vicinity of the solution.

The conditions which must be satisfied to have a cyclic path are represented in vector form as

$$\Psi = \begin{bmatrix} Z_{i_f} - Z_{i_0} \quad ; \; i = 1,\ldots,6 \; ; \; i \neq 3 \; ; \; i \neq j \\ Z_{3_f} - 0 \\ Z_{j_f} - \text{const} \end{bmatrix} . \qquad (7.1)$$

The special conditions imposed on the 3^{rd} and j^{th} elements of Ψ are necessary to satisfy the uniqueness requirement of the solution. Specifying $Z_{3_0} = 0$ implies that the path starts at $Y_0 = 0$. This specifies the point on the path to which the shooting method converges. $Y_0 = 0$

happens twice in a simple cycle, once at the maximum altitude of the cycle and once at the minimum altitude of the cycle. All results presented in this report are for $\gamma_0 = 0$ at the maximum altitude.

As was seen in Section VI, there are continuous families of initial conditions which produce cyclic paths. Specifying $Z_{j_0} = \text{const}$ causes the shooting method to converge to a particular solution on the family. It should be noted that specifying $Z_{j_0} = \text{const}$ and $\bar{x}_f$ free is equivalent to specifying $Z_{j_f} = Z_{j_0}$ and $\bar{x}_f = \text{const}$. Thus, when the shooting method converges and a cyclic path is found, all the first variation necessary conditions for the fixed final range problem stated in Section IV will be satisfied. Points on the family where H = J will satisfy all the first variation necessary conditions for the free final range problem. To better illustrate the role that j plays on Ψ, Ψ for j = 5 is presented below :

$$\Psi = \begin{bmatrix} Z_{1_f} - Z_{1_0} \\ Z_{2_f} - Z_{2_0} \\ Z_{3_f} \\ Z_{4_f} - Z_{4_0} \\ Z_{5_f} - \text{const} \\ Z_{6_f} - Z_{6_0} \end{bmatrix} .$$

The algorithm for selecting j will be presented in Section VIII.

From one iteration to the next, the magnitude of Ψ should decrease,

$$\Psi^{n+1} - \Psi^{n} = - \beta \Psi^{n} = \delta \Psi^{n}(Z_0, Z_f) \quad , \tag{7.2}$$

where Ψ^{n} is Ψ for the n^{th} iteration, Ψ^{n+1} is Ψ for the $n+1^{th}$ iteration, and the variable β is adjusted to vary the speed of convergence. Fast convergence near a solution is obtained by setting $\beta = 1$. Farther away from the solution, it is desired to stay within the linear assumption of the shooting method. This is done by chosing β as $0 < \beta < 1$.

Take the variation indicated in Equation (7.2) :

$$- \beta \Psi = \Psi_{Z_0} \delta Z_0 + \Psi_{Z_f} \delta Z_f \quad . \tag{7.3}$$

Since the 3^{rd} and j^{th} initial conditions are constant, $\delta Z_{3_0} = 0$ and $\delta Z_{j_0} = 0$. Define a new vector $\overline{\delta Z_0}$ which contains 4 elements and is obtained by removing the 3^{rd} and j^{th} elements from δZ_0, and a new matrix $\overline{\Psi}_{Z_0}$ which is Ψ_{Z_0} with the 3^{rd} and j^{th} columns removed. Equation (7.3) then becomes

$$- \beta \Psi = \overline{\Psi}_{Z_0} \overline{\delta Z_0} + \Psi_{Z_f} \delta Z_f \quad . \tag{7.4}$$

Note that

$$\delta Z = \tilde{\delta} Z + Z' \overline{\delta x} \quad ,$$

$$\delta\bar{z}_0 = \tilde{\delta}\bar{z}_0 \quad , \tag{7.5}$$

$$\delta z_f = \tilde{\delta} z_f + z'_f \, \delta\bar{x}_f \quad , \tag{7.6}$$

$$\tilde{\delta} z_f = \bar{\phi} \, \tilde{\delta}\bar{z}_0 \quad , \tag{7.7}$$

where $\tilde{\delta}\bar{z}_0$ is $\tilde{\delta} z_0$ with the 3^{rd} and j^{th} elements removed, and $\bar{\phi}$ is $\phi(\bar{x}_f, 0)$ with the 3^{rd} and j^{th} columns removed. Substitute Equations (7.5) through (7.7) into Equation (7.4). The result is

$$-\beta\psi = \psi_{z_f} z'_f \, \delta\bar{x}_f + (\psi_{z_f} \bar{\phi} + \bar{\psi}_{z_0}) \, \tilde{\delta}\bar{z}_0 \quad ,$$

which can be expressed in matrix form as

$$[\psi_{z_f} z'_f \mid (\psi_{z_f} \bar{\phi} + \bar{\psi}_{z_0})] \begin{bmatrix} \delta\bar{x}_f \\ \tilde{\delta}\bar{z}_0 \end{bmatrix} = -\beta\psi \quad . \tag{7.8}$$

From Equation (7.1), note that

$$\psi_{z_f} = I \quad , \tag{7.9}$$

$$\bar{\psi}_{z_0} = -\bar{I} \quad , \tag{7.10}$$

where $\bar{I}$ is I with the 3^{rd} and j^{th} columns removed. Substitute Equations (7.9) and (7.10) into Equation (7.8). The result is the linear system used in the shooting method for this investigation :

$$[Z'_f \mid (\bar{\phi} - \bar{I})] \begin{bmatrix} \delta\bar{x}_f \\ \delta\bar{Z}_0 \end{bmatrix} = - \mid B \Psi \quad . \tag{7.11}$$

To calculate the perturbations $\delta\bar{x}_f$ and $\delta\bar{Z}_0$, the linear system of Equation (7.11) must be solved. The vector Z'_f is 6 by 1 and the matrix $(\bar{\phi} - \bar{I})$ is 6 by 4. The left hand side matrix of Equation (7.11) is 6 by 5. Since the linear system is not square, it is solved in a least square sense using the pseudo-inverse.

The algorithm for obtaining a cycle is

1) Initialize :

   Z_0 - guess,

   $\bar{x}_f$ - guess,

   $\mid B$ - set,

   j - set.

2) Calculate Z_f and ϕ using algorithm of Section 5.7.

3) Calculate Ψ.

4) If convergence is achieved, go to 6.

5) Convergence not achieved :

   form and solve linear system of Equation (7.11),

   update initial conditions and final range,

   $Z_0 = Z_0 + \bar{I}\ \delta\bar{Z}_0$,

   $\bar{x}_f = \bar{x}_f + \delta\bar{x}_f$,

   go to 2.

6) Convergence achieved :

stop.

7.2 Shooting Method Performance

The shooting method presented above has been used almost exclusively during this investigation. This method has worked very well. When Z_0 and $\bar{x}_f$ are within 2 to 3 significant digits of the solution, it takes only about 3 iterations to find the solution to 10 digits. The space around a solution is highly non-linear. This makes convergence very difficult or impossible when the guess on Z_0 and $\bar{x}_f$ is not within 2 digits of the solution. Because of this, the first cycle is difficult to find. Once one cycle is found, an algorithm exists to predict Z_0 and $\bar{x}_f$ for a neighboring cycle. This algorithm will be presented in Section VIII.

Section VIII

Tracing Families

This Section describes the algorithms used for tracing a family of initial conditions. The second order generalized eigenvector used to start the family trace is described first. Finally, an extrapolation routine used to trace the family after several points on the family have been obtained is presented.

8.1 Eigenvector Direction

In [9], Speyer states that the second order generalized eigenvector points in the direction of a family of cyclic paths. Therefore, given one cycle, the second order generalized eigenvector, s, can be used to predict the initial conditions of a neighboring cycle. Equation (6.23) is rearranged to give a more useful form of s :

$$s = \alpha_1 (V_1 + \alpha_2 V_2) \quad , \tag{8.1}$$

where,

$$V_1 = \begin{bmatrix} -A_{11}^{-1} A_{11}^{-1} A_{12} \\ 0 \end{bmatrix} \quad ,$$

$$V_2 = \begin{bmatrix} -A_{11}^{-1} A_{12} \\ I \end{bmatrix} \quad ,$$

$$\alpha_1 = p_2 \quad ,$$

$$\alpha_2 = \frac{s_2}{p_2} \quad .$$

In equation (8.1), it is seen that α_2 affects how V_1 and V_2 are linearly combined, and α_2 affects the length of s. The scalars α_1 and α_2 are chosen to take full advantage of the non-uniqueness of eigenvectors. The s vector is used to perturb the initial conditions, Z(0), in the direction of a neighboring cycle. In this report, the only initial conditions of interest are those where $\gamma_0 = 0$ at the maximum altitude of the cycle. Thus, it is desired to have the γ perturbation of s equal to 0, $s_3 = 0$. This is obtained by choosing $\alpha_2 = -V_{1_3}/V_{2_3}$ where V_{1_3} and V_{2_3} are the 3^{rd} components of V_1 and V_2 respectively. The scalar α_1 is chosen such that the perturbation vector s is a certain length. Notice that the sign of α_1 is used to control which way on the family the tracing is done. By changing the sign of α_1, the direction of the perturbation is changed.

It is interesting to note that V_2 is proportional to the initial derivative vector. The V_1 vector contains perturbation components in both the family direction and the initial derivative direction. By choosing α_2 correctly, $\alpha_2 V_2$ is used to take the initial derivative direction out of V_1 leaving only the desired family direction.

8.2 Extrapolation Routine

Using the second order generalized eigenvector to trace the families is very inefficient. The calculation of s involves a matrix

inversion and 3 matrix multiplications. When several points on the family are found, an extrapolation routine is used to predict new neighboring cycles.

The extrapolation routine first chooses one of the 6 states as the independent variable for the extrapolation. The other 5 states are then extrapolated individually by curve fitting the state against the independent variable. The result is the prediction of a neighboring cycle. Experience has shown fitting a 3^{rd} order curve through the last 4 family points works well.

Suppose the curve in Figure 6 is Z_k vs. Z_i for a portion of the family. In region a, Z_k would be chosen as the independent variable for the extrapolation because Z_i is a one-to-one function of Z_k. In region b, Z_i would be chosen as the independent variable for the same reasoning.

The independent variable chosen for the extrapolation is also used as j for the shooting method in Section VII. The reason for this is seen by refering to point c in Figure 6. If c is the prediction of a neighboring cycle, the shooting method will attempt to close the prediction to the family. If j = k, the shooting method will not be able to close the prediction. However, if j = i, closure will be achieved.

The size of the extrapolation step is controlled such that the prediction of the neighboring cycle closes to the family in a certain number of iterations of the shooting method. If the shooting method

takes more iterations than specified, the extrapolation step is scaled down for the next extrapolation. Similarly, if the shooting method takes less iterations than specified, the extrapolation step is scaled up. Experience has shown the shooting method should converge in two iterations.

Section IX

Discussion of Families

This section starts by presenting the families generated using the methods of the previous sections. A comparison between the steady state and periodic cruise is presented next. Finally, phase plane diagrams for a particular cycle are presented to show the character of a cycle.

9.1 Spherical Earth Family

Figures 7a through 7g show the spherical earth family. Figures 7a through 7f are, in order: $\bar{h}$ vs. M, $\lambda_{\bar{h}}$ vs. M, λ_M vs. M, λ_γ vs. M, J and H vs. M, and $\bar{x}_f$ vs M for the family. Figure 7g is a_2 vs. a_1, stability coefficients, for the family. The symbols on each figure are used to relate a particular family point on one figure to the same family point on another figure. Notice the cusp at $M \simeq 2$. All the state variables have this cusp except $\lambda_{\bar{h}}$.

The points on the family satisfy all the first variation necessary conditions for the fixed final range problem. The only first variation necessary condition not satisfied for the free final range problem is H = J. Refer to Figure 7e which is J and H vs. M. There are 2 points on the family where H = J, one at M = 2.58 and another at M = 3.77. In [10], Speyer developes a second variation sufficient for non-optimality : that there exist distinct eigenvalues on the unit circle. Refer to Figure 7g to see the cycle at M = 3.77 has distinct eigenvalues

on the unit circle and therefore cannot be an optimal solution. The cycle at M = 2.58 does not have any distinct eigenvalues on the unit circle. [5] and [9] present a second variation sufficient condition for optimality : that a real valued Riccati matrix be periodic and remain finite. This test should be applied to the M = 2.58 cycle to confirm that the cycle satisfies all the second variation conditions for a relative minimum.

9.2 Flat Earth Family

Figures 8a through 8h show the flat earth family. Although this family has little practical importance, it is interesting theoretically. The flat earth family has the same cusp displayed by the spherical earth.

By comparing Figures 7b through 7d with 8b through 8d, it is seen that the shape of the flat earth and spherical earth λ's are very similar. Figure 8e and 8f are J and H vs. M for the flat earth family. Figure 8f is an expanded plot of the flat portion of Figure 8e. Walker [11] stated that first order optimization techniques failed to converge. The flatness in Figure 8e may be the reason for this. There are two cycles where H = J. The one at M = 6.36 has the distinct eigenvalues off the unit circle. This cycle is a possible minimum for the flat earth free final range problem. The Riccati matrix test should also be applied to this cycle.

9.3 Comparison of Periodic and Steady State

Figure 9a is dimensional altitude vs. Mach number on the spherical earth family for both the periodic and steady state solutions. Recall that the altitude for the periodic solution is the maximum altitude.

Figures 9b and 9c are two different comparisons of performance index for the spherical earth. Figure 9b is J vs. M. The periodic solutions show an improvement over steady state of about 4% at M = 2 to about 2% at M = 8. Figure 9c is J vs. minimum specific energy, energy per unit weight, of the cycle. The justification for comparing J vs. minimum specific energy of the cycle follows. Since a SCRAM engine does not have turbines, it cannot develop any static thrust. Some type of assisted launch could be used to get the hypercruiser flying. The launch assist system is limited to the amount of energy it is able to impart to the hypercruiser. It is true that the SCRAM engine can be used after launch to increase the energy of the hypercruiser, but this can be considered to be part of the launch. Given that a certain amount of energy can be imparted to the hypercruiser to establish cruise, what type of cruise is best? The periodic cruise shows an improvement over steady state which is roughly constant at about 4.5%.

Figures 10a and 10b show comparisons for the flat earth case. The minimum specific energy comparison is not shown because J_{ss} is constant for the flat earth. The improvement of periodic over steady state is roughly constant at about 4%.

9.4 Phase Plane

Figures 11a through 11g are plots of a particular cycle at M = 8.06 on the spherical earth family. Figure 11a is dimensional altitude vs. M. This cycle has the best performance index of any found to date, yet does not satisfy the first variation necessary conditions for the free final range problem. Figures 11a through 11e are phase plane plots which show the magnitude of oscillation in the state variables for the cycle. Of particular interest is Figure 11a. This cycle oscilates in altitude between about 90,000 ft and 130,000 ft, and in Mach number between about 7.45 and 8.15. Another interesting fact is the maximum specific energy of the cycle is approximately twice that of the minimum specific energy of the cycle.

Figure 11f and 11g show the control history of the cycle. For this vehicle, $C_{L_{E_{max}}} = .157$. The C_L control for this cycle is operating around this value. The corners in the C_L history are caused by the thrust switching.

This cycle at M = 8.06 has a peculiar property. Normally, $(\Phi - I)$ is rank 5. At this point on the family, $(\Phi - I)$ has rank 4 and still only 2 unity eigenvalues. This indicates that the Jordan box containing the 2 unity eigenvalues has disappeared. This is believed to be caused by the fact that $\partial \bar{x}_f / \partial H = 0$ at this point on the family.

Section X

Conclusions

Families of cyclic paths are shown which result in better cruise performance than steady state. One point on the spherical earth family and one point on the flat earth family are presented as possible relative minimums for the free final range problem. The Riccati matrix test should be done to verify this. The possible relative minimum on the spherical earth family is of particular interest since M = 2.5 is attainable with current technology.

The emphasis in this report is on the development of numerical algorithms to be used in the investigation of periodic optimal control problems. Walker [11] describes a more realistic SCRAM engine model. Future work should incorporate this model to see how the results are affected.

This report showed only one family for each model. Other families exist. The point where two families cross is called a bifurcation point. Appendix B contains an explanation of the bifurcation point and a possible numerical algorithm for finding crossing families. This algorithm has not been implemented. These other families may result in better cruise performance.

Appendix A

A Matrix Elements

This Appendix contains the elements of A used in the transition matrix differential equation, Equation (5.18).

$$A_{11} = 0$$

$$A_{12} = 0$$

$$A_{13} = \frac{1}{\cos^2 \gamma}$$

$$A_{14} = 0$$

$$A_{15} = 0$$

$$A_{16} = 0$$

$$A_{21} = -\frac{g F^2 C_2 D}{M a^2 W \cos \gamma}$$

$$A_{22} = -\frac{g F (T - D - W \sin \gamma}{M^2 a^2 W \cos \gamma} - \frac{g F p k b^2 C_{D_0}}{a^2 W \cos \gamma}$$

$$A_{23} = \frac{g F \sin \gamma (T - D - W \sin \gamma)}{M a^2 W \cos^2 \gamma} - \frac{g F}{M a^2}$$

$$A_{24} = 0$$

$$A_{25} = \frac{\rho_\gamma g F L}{\rho_M^2 M^2 a^2 W \cos \gamma}$$

$$A_{26} = -\frac{g\ F\ L}{\lambda_M\ M^2\ a^2\ W \cos \gamma}$$

$$A_{31} = \frac{g\ F^2\ C_2\ L}{M^2\ a^2\ W \cos \gamma} - \frac{1}{(\bar{R}_0 + \bar{h})^2}$$

$$A_{32} = \frac{2\ g\ F}{M^3\ a^2} - \frac{g\ F\ L}{M^3\ a^2\ W \cos \gamma}$$

$$A_{33} = \frac{g\ F\ L \sin \gamma}{M^2\ a^2\ W \cos \gamma}$$

$$A_{34} = 0$$

$$A_{35} = -\frac{g\ F\ L}{M^2\ a^2\ W\ \lambda_M \cos \gamma}$$

$$A_{36} = \frac{g\ G\ L}{M^2\ a^2\ W\ \lambda_\gamma \cos \gamma}$$

$$A_{41} = \frac{\lambda_M\ g\ F^3\ C_2^2\ D}{M\ a^2\ W \cos \gamma} - \frac{\lambda_\gamma\ g\ F^3\ C_2^2\ L}{M^2\ a^2\ W \cos \gamma}$$

$$- \frac{2\ \lambda_\gamma}{(\bar{R}_0 + \bar{h})^3}$$

$$A_{42} = -\frac{\lambda_M\ g\ F^2\ C_2\ D}{M^2\ a^2\ W \cos \gamma} + \frac{\lambda_M\ g\ F^2\ C_2\ p\ k\ b^2\ C_{D_0}}{a^2\ W \cos \gamma}$$

$$+ \frac{\lambda_\gamma\ g\ F^2\ C_2\ L}{M^3\ a^2\ W \cos \gamma}$$

$$A_{43} = \frac{\lambda_M\ g\ F^2\ C_2\ D \sin \gamma}{M\ a^2\ W \cos^2 \gamma} - \frac{\lambda_\gamma\ g\ F^2\ C_2\ L \sin \gamma}{M^2\ a^2\ W \cos^2 \gamma}$$

$$A_{44} = 0$$

$$A_{45} = \frac{g F^2 C_2 D}{M a^2 W \cos \gamma}$$

$$A_{46} = - \frac{g F^2 C_2 L}{M^2 a^2 W \cos \gamma} + \frac{1}{(\bar{R}_0 + \bar{h})^2}$$

$$A_{51} = \frac{\rho_M g F^2 C_2 D}{M^2 a^2 W \cos \gamma}$$

$$A_{52} = - \frac{\rho_M g F p k b^2 C_{D_0}}{M a^2 W \cos \gamma} - \frac{2 \rho_M g F (T - D - W \sin \gamma)}{M^3 a^2 W \cos \gamma}$$

$$- \frac{2 \rho_\gamma g F L}{M^4 a^2 W \cos \gamma} + \frac{6 \rho_\gamma g F}{M^4 a^2}$$

$$A_{53} = \frac{\rho_M g F [(T - D) \sin \gamma - W]}{M^2 a^2 W \cos^2 \gamma}$$

$$+ \frac{\rho_M g F p k b^2 C_{D_0} \sin \gamma}{a^2 W \cos^2 \gamma} + \frac{\rho_\gamma g F L \sin \gamma}{M^3 a^2 W \cos^2 \gamma}$$

$$A_{54} = 0$$

$$A_{55} = \frac{g F (T - D - W \sin \gamma)}{M^2 a^2 W \cos \gamma} + \frac{g F p k b^2 C_{D_0}}{a^2 W \cos \gamma}$$

$$A_{56} = \frac{g F L}{M^3 a^2 W \cos \gamma} - \frac{2 g F}{M^3 a^2}$$

$$A_{61} = \frac{\lambda_M \, g \, F^2 \, C_2 \, D \sin \gamma}{M \, a^2 \, W \cos^2 \gamma} - \frac{\lambda_\gamma \, g \, F^2 \, C_2 \, L \sin \gamma}{M^2 \, a^2 \, W \cos^2 \gamma}$$

$$A_{62} = \frac{\lambda_M \, g \, F \, [(T - D + p \, k \, b^2 \, M^2 \, C_{D_0}) \sin \gamma - W]}{M^2 \, a^2 \, W \cos^2 \gamma}$$

$$+ \frac{\lambda_\gamma \, g \, F \, L \sin \gamma}{M^3 \, a^2 \, W \cos^2 \gamma}$$

$$A_{63} = [- \frac{\dot{V}_T}{a} - \frac{\lambda_M \, g \, F(T - D)}{M \, a^2 \, W} - \frac{\lambda_\gamma \, g \, F \, L}{M^2 \, a^2 \, W}][\frac{2 \sin^2 \gamma}{\cos^3 \gamma} + \frac{1}{\cos \gamma}]$$

$$- [\frac{\lambda_h}{h} - \frac{\lambda_M \, g \, F}{M \, a^2}] \frac{2 \sin \gamma}{\cos^3 \gamma}$$

$$A_{64} = - \frac{1}{\cos^2 \gamma}$$

$$A_{65} = - \frac{g \, F \, (T - D) \sin \gamma}{M \, a^2 \, W \cos^2 \gamma} + \frac{g \, F}{M \, a^2 \cos^2 \gamma}$$

$$A_{66} = - \frac{g \, F \, L \sin \gamma}{M^2 \, a^2 \, W \cos^2 \gamma}$$

Appendix B

Bifurcation Points

A bifurcation point is where two families cross. At a bifurcation point the cycles for both families are identical. Several interesting things happen to the transition matrix at a bifurcation. First, the transition matrix acquires two extra unity eigenvalues to make a total of four. Recall that this is precisely the condition on the line represented by Equation (6.13) in the a_1,a_2 plane. This line is therefore referred to as the single period bifurcation line. The line in the a_1,a_2 plane represented by Equation (6.12) is refered to as the double period bifurcation line. The reason for this can be understood by examining what happens to the eigenvalues of Φ over multiple periods. Define Φ' to be the transition matrix evaluated over a single period and λ' to be its eigenvalues. Over two periods the transition matrix is $\Phi'' = \Phi'\Phi'$ and the eigenvalues of Φ'' are $\lambda'' = (\lambda')^2$. If a cycle is on the double period bifurcation line it has two eigenvalues at -1. Over two periods these eigenvalues become $(-1)^2 = 1$. A line in the a_1,a_2 plane can be identified as the i^{th} period bifurcation line for any integer i.

The second interesting thing to happen to Φ at a bifurcation is the rank of $(\Phi - I)$ drops from the normal 5 to 4. This indicates that the Jordon form of Φ acquires a second off-diagonal 1. We assume that the Jordon form is

$$\begin{bmatrix} \lambda & & & & \\ & 1 & & & \\ & \lambda & & & \\ & & 1 & 1 & \\ & & & 1 & \\ & & & & 1 & 1 \\ & & & & & 1 \end{bmatrix} \qquad \text{(B.1)}$$

If this is the case then there are two primary eigenvectors associated with two of the unity eigenvalues and two second-order generalized eigenvectors associated with the other unity eigenvalues.

It should be mentioned that the fact that $\underline{\delta}$ acquires two extra unity eigenvalues does not guarantee that the rank of $(\underline{\delta} - I)$ drops. Figure 7g shows that the spherical earth family crosses the single period bifurcation line twice. The rank of $(\underline{\delta} - I)$ does not drop at either of these points. This requires the Jordon form of $\underline{\delta}$ to be

$$\begin{bmatrix} \lambda & & & & \\ & 1 & & & \\ & \lambda & & & \\ & & 1 & 1 & \\ & & & 1 & 1 \\ & & & & 1 \end{bmatrix} \qquad \text{(B.2)}$$

at these points. Figure 7g also shows that the spherical earth family crosses the double period bifurcation line three times. One of these points was selected and evaluated over two periods and the rank dropped to four.

Figure 12 shows a bifurcation in the $\bar{h}$ vs. M plane for the spherical earth family. The new family shown in Figure 12 was found by doing a crude search around the bifurcation point. It would be desir-

able to find a more systematic and efficient method to break off of a bifurcation point. The author has not implemented such a method, but following are some ideas on the subject.

Equation (6.22) is the equation for the primary eigenvectors. Since $(\mathbf{\Phi} - I)$ is rank 4, A_{11} is 4 by 4, A_{12} is 4 by 2, and p_2 is a 2 vector. The primary eigenvector equation can be written as

$$p = V_1 \alpha_1 + V_2 \alpha_2 \quad , \tag{B.3}$$

where V_1 and V_2 are 6 vectors and α_1 and α_2 are scalars. Along the family, it has been shown that Z'(0) is a primary eigenvector. A test was done to test the linear dependence of Z'(0) on V_1 and V_2 by calculating the determinant of the Grammian matrix [1]. The determinant was zero indicating that Z'(0) is linearly dependent on V_1 and V_2 and therefore is a primary eigenvector.

Equation (6.23) is the equation for the second-order generalized eigenvector and can be represented as

$$s = V_1 \alpha_1 + V_2 \alpha_2 + V_3 \alpha_3 + V_4 \alpha_4 \quad , \tag{B.4}$$

where the V's and α's are different vectors and scalars from those in Equation (B.3). If s is used as the family direction, Equation (B.4) indicates that a search in a four-dimensional subspace of the six-dimensional state space is necessary at a bifurcation point. This four-dimensional search can be further reduced. Recall that for the hypercruiser problem the only families of interest are those where

$y_0 = 0$. Thus, specifying $s_3 = 0$ reduces the search to three dimensions. The search can be reduced further by specifying the magnitude of s. By specifying $|s| = \text{const}$, the search is reduced to two dimensions.

One further reduction will be discussed based on the premise that the correct search direction is the second-order generalized eigenvector associated with Z'(0) as the primary eigenvector, the search can be reduced to a one-dimensional search. To better illustrate this point, the solution to the second-order generalized eigenvector can be written in another form:

$$s = \begin{bmatrix} A_{11}^{-1} \\ 0 \end{bmatrix} p_1 + \begin{bmatrix} -A_{11}^{-1} A_{12} \\ I \end{bmatrix} s_2 \quad , \tag{B.5}$$

$$= \begin{bmatrix} A_{11}^{-1} \\ 0 \end{bmatrix} \begin{bmatrix} -A_{11}^{-1} A_{12} \end{bmatrix} p_2 + \begin{bmatrix} -A_{11}^{-1} A_{12} \\ I \end{bmatrix} s_2 \quad . \tag{B.6}$$

Equation (B.6) shows that if p_1 (in Equation (B.5)) is to be in the direction of Z'(0), the two elements of p_2 are not independent. This fact combined with the two previous reductions gives a one-dimensional search. This is a big improvement over the six-dimensional brute force search of the state space.

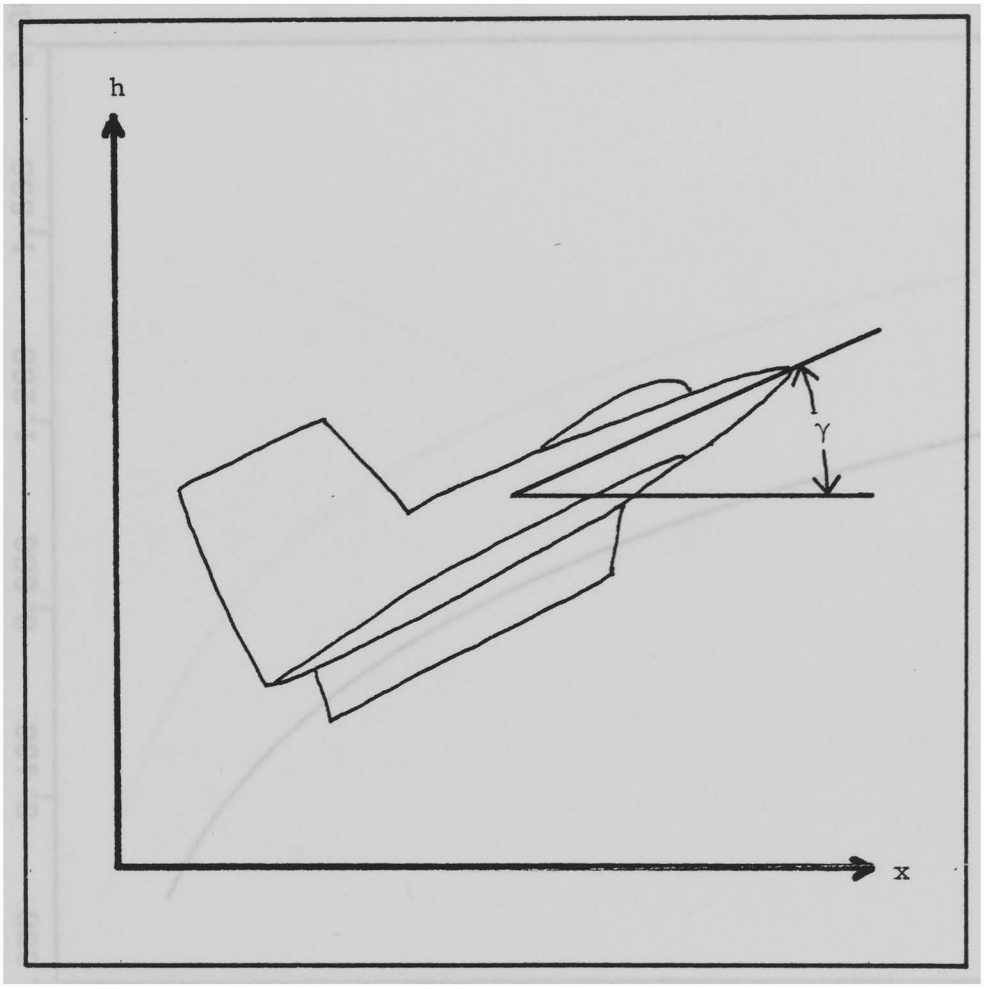

Figure 1 Coordinate System.

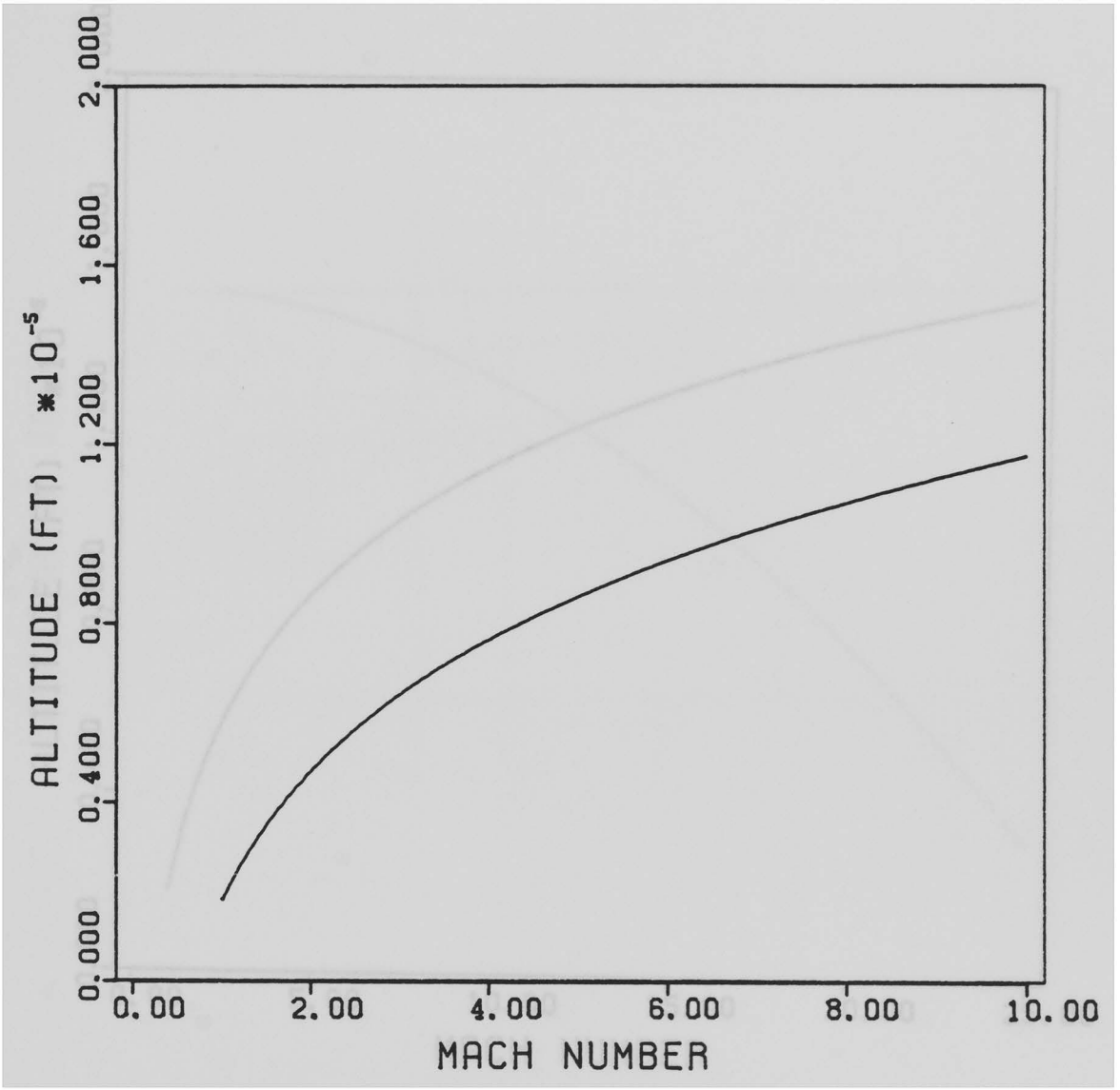

Figure 2a Steady State, Spherical Earth.

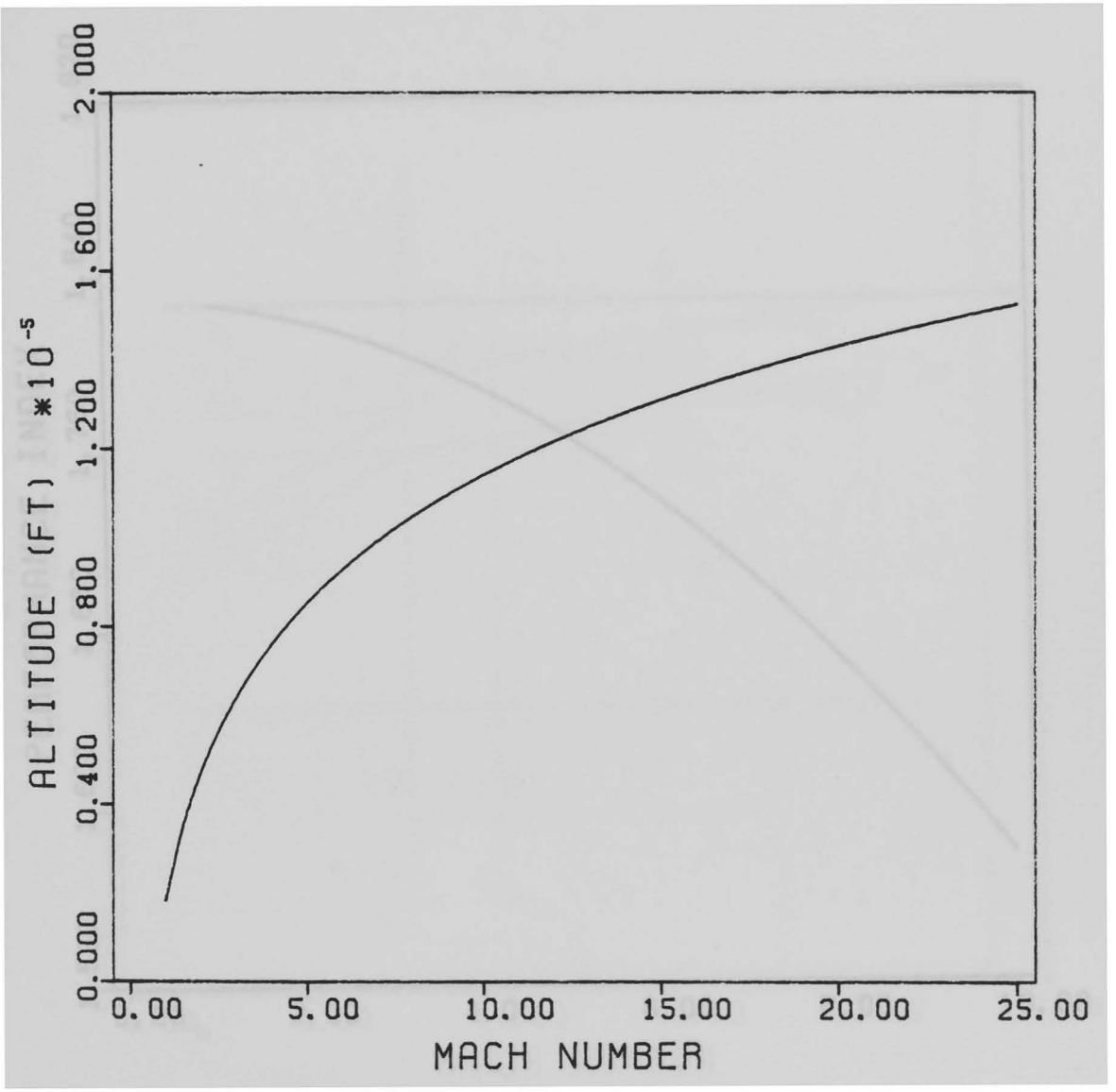

Figure 2b Steady State, Flat Earth.

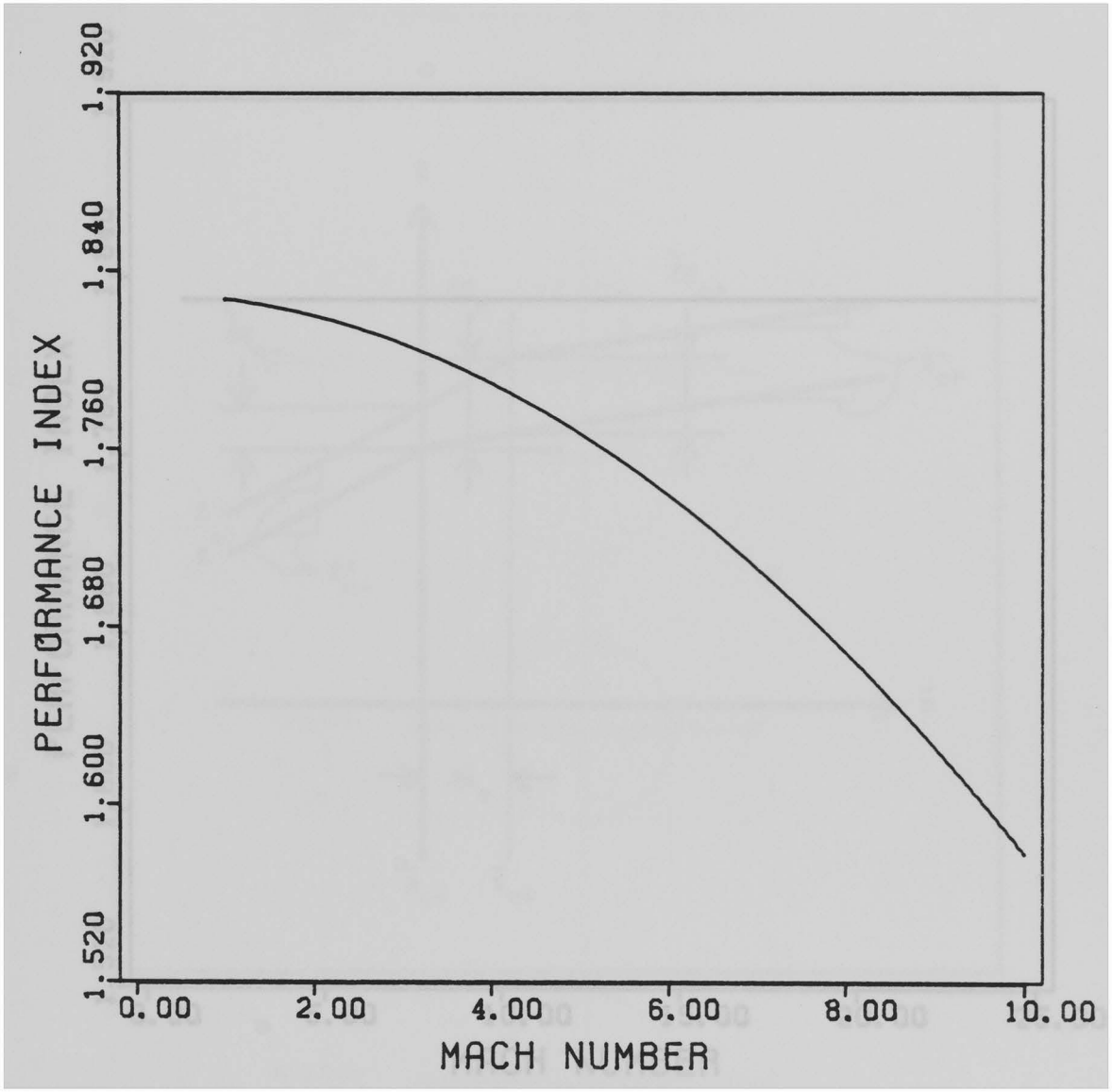

Figure 2c Steady State, Spherical Earth.

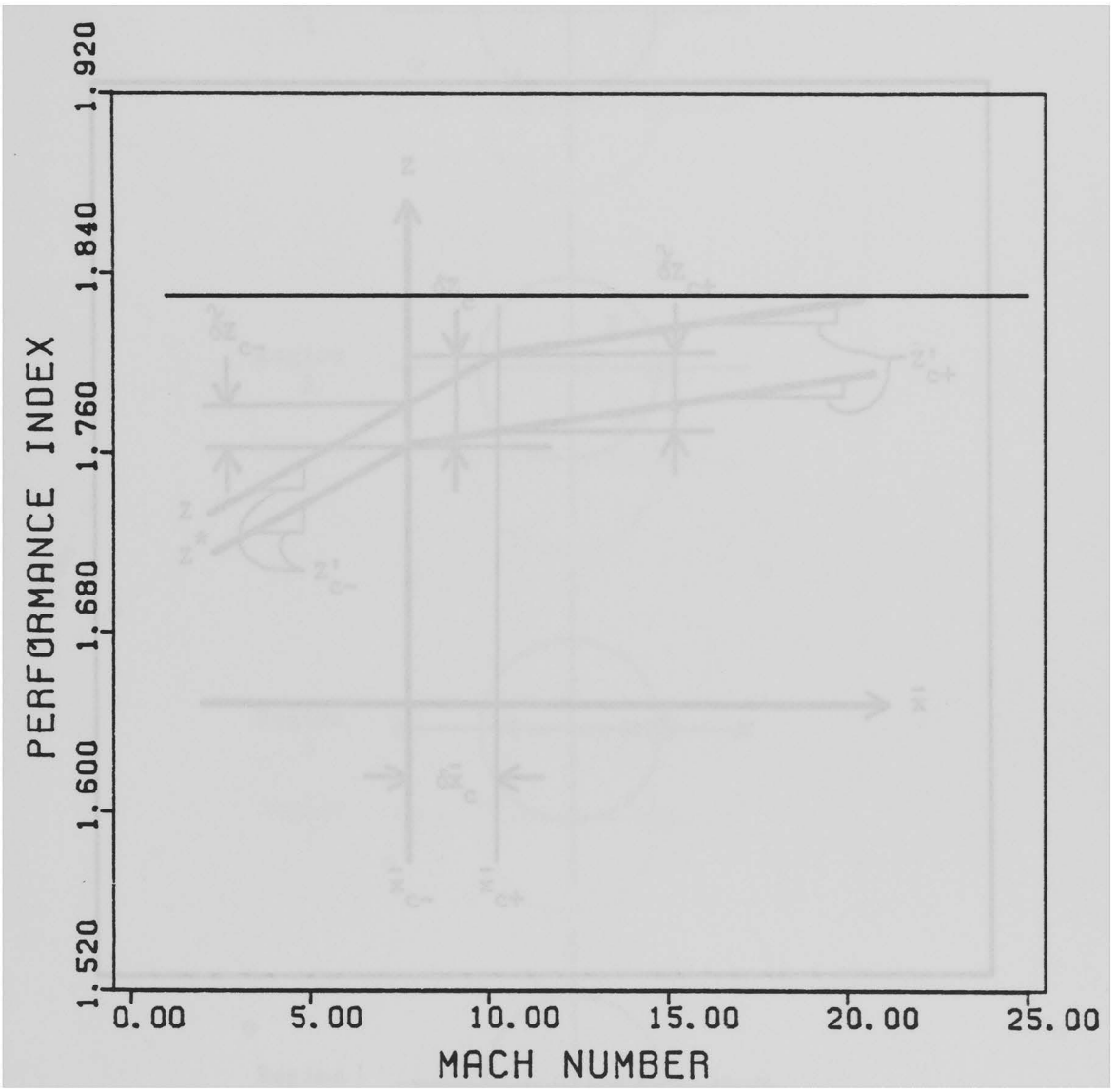

Figure 2d Steady State, Flat Earth.

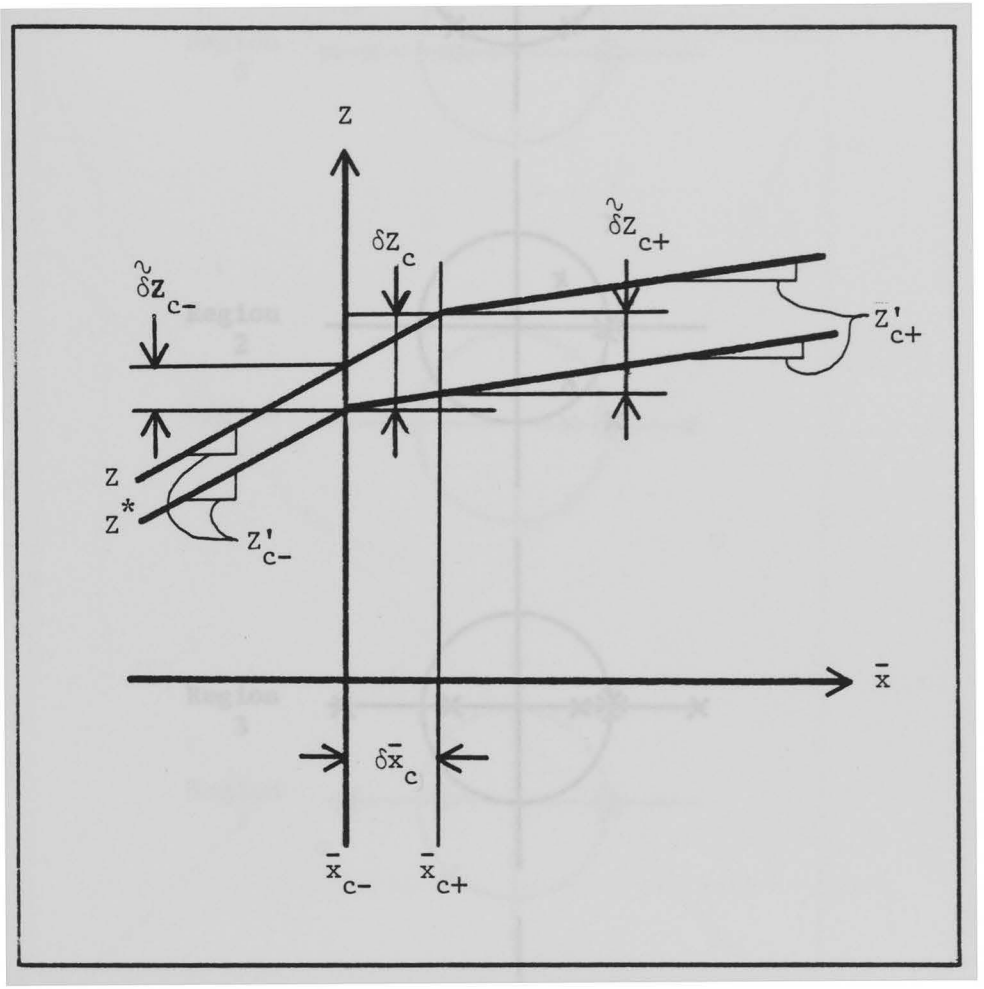

Figure 3 Notation for Jump in Transition Matrix.

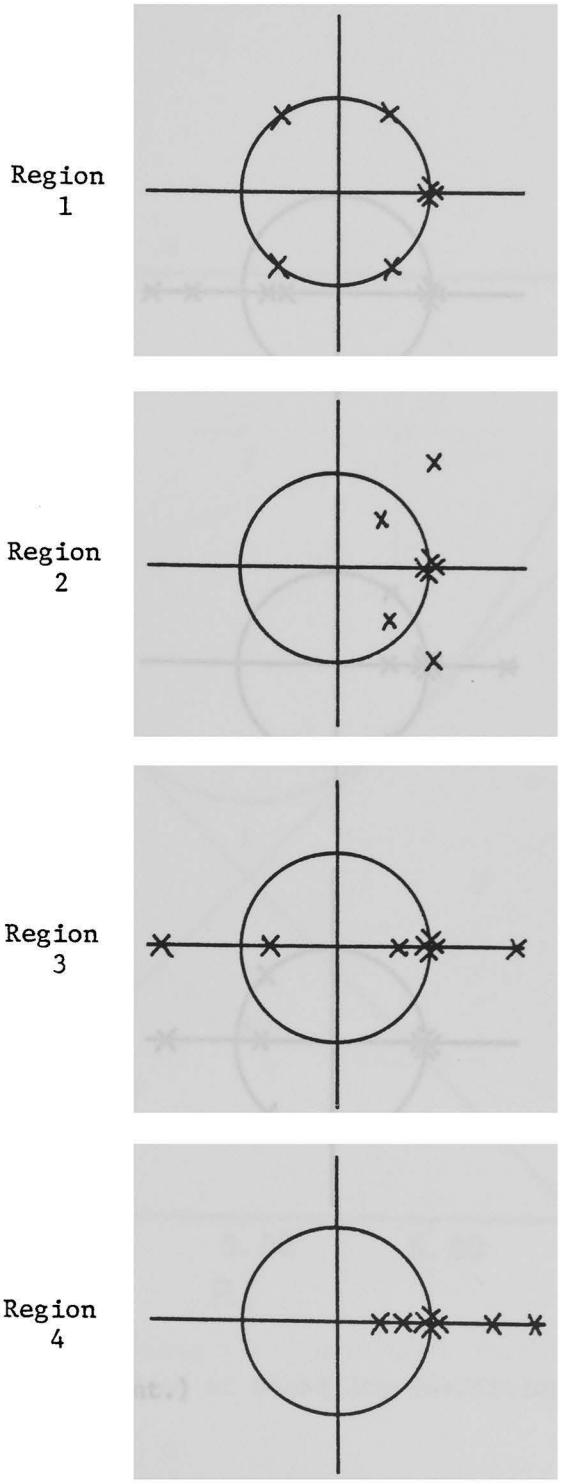

Figure 4 Possible eigenvalue configurations.

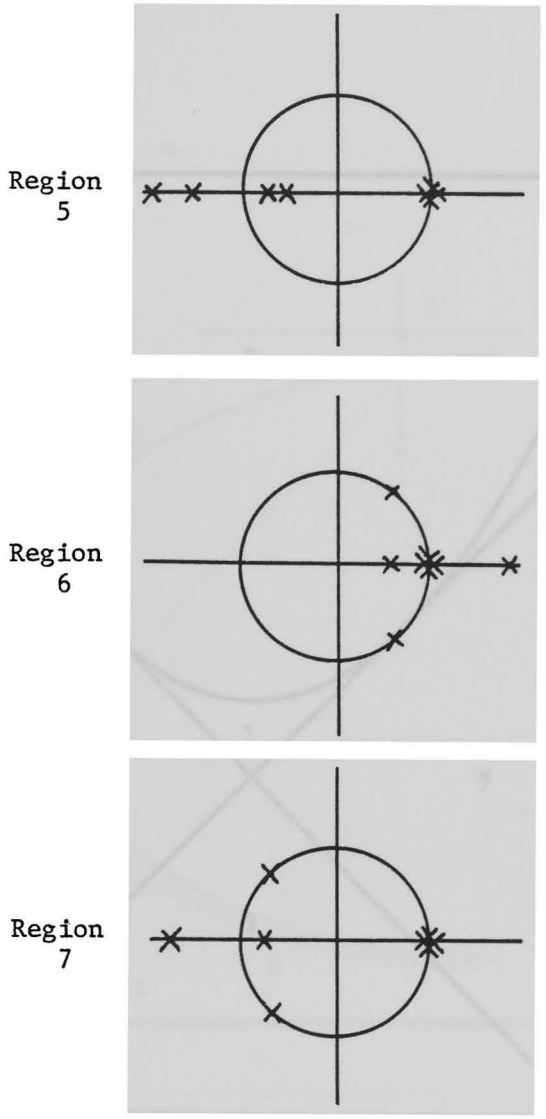

Figure 4 (cont.)

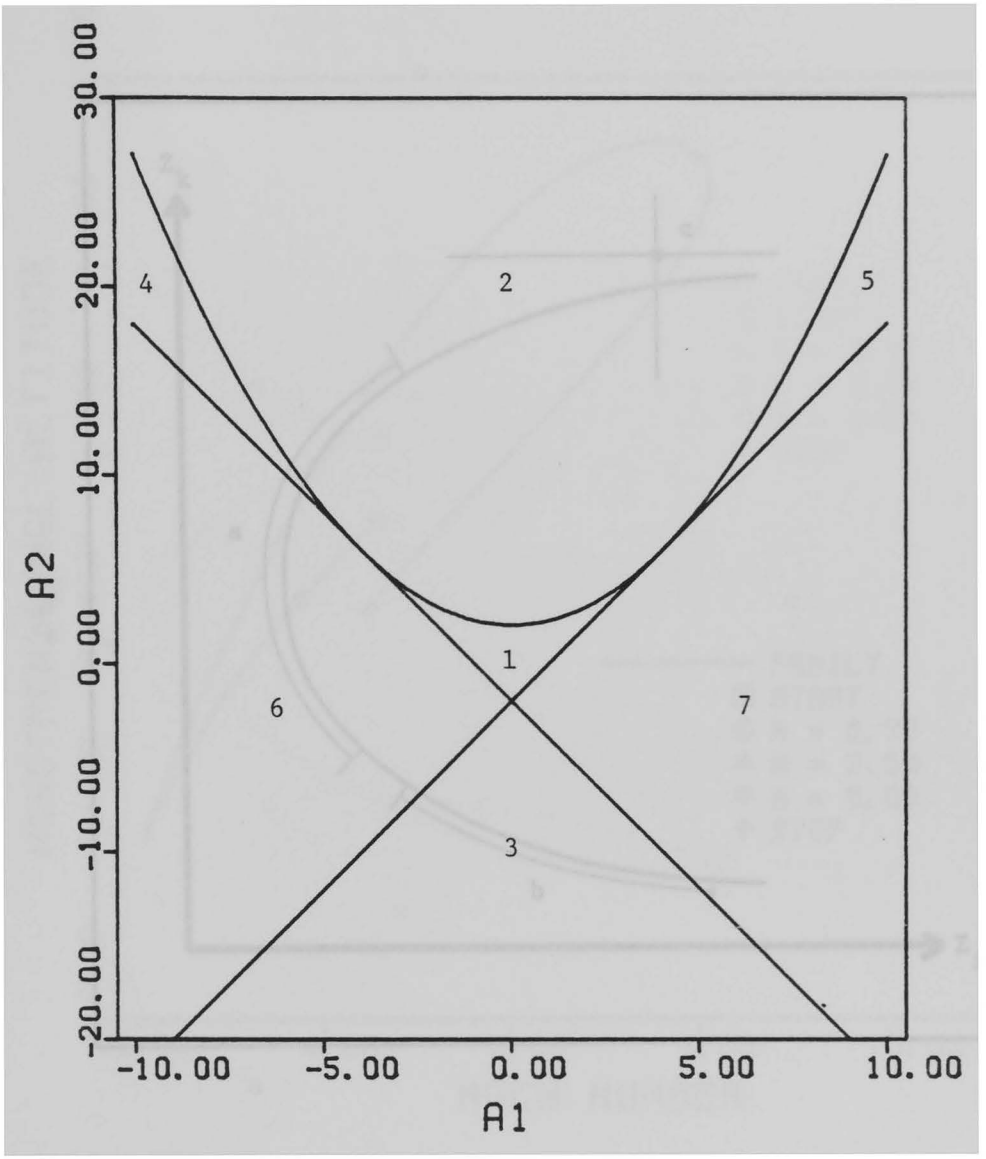

Figure 5 Regions of Stability Coefficients.

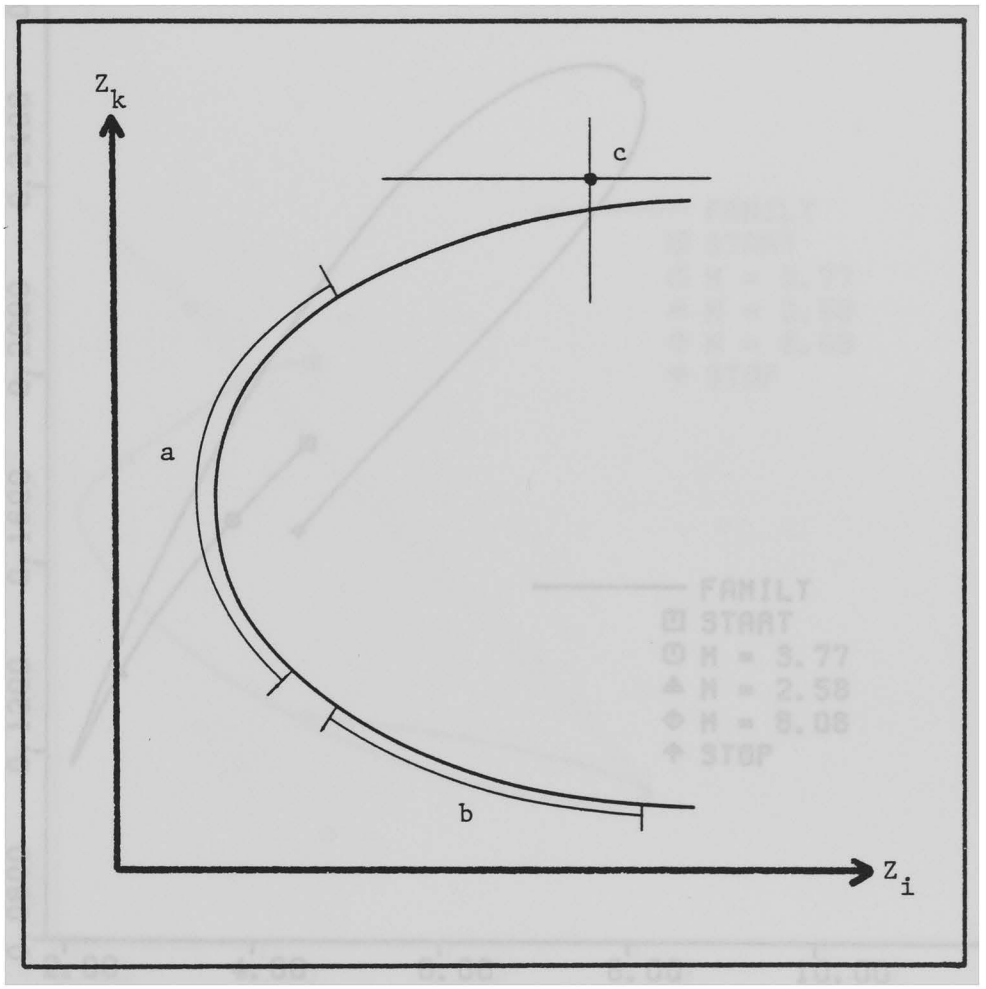

Figure 6 Choosing the Independent Variable.

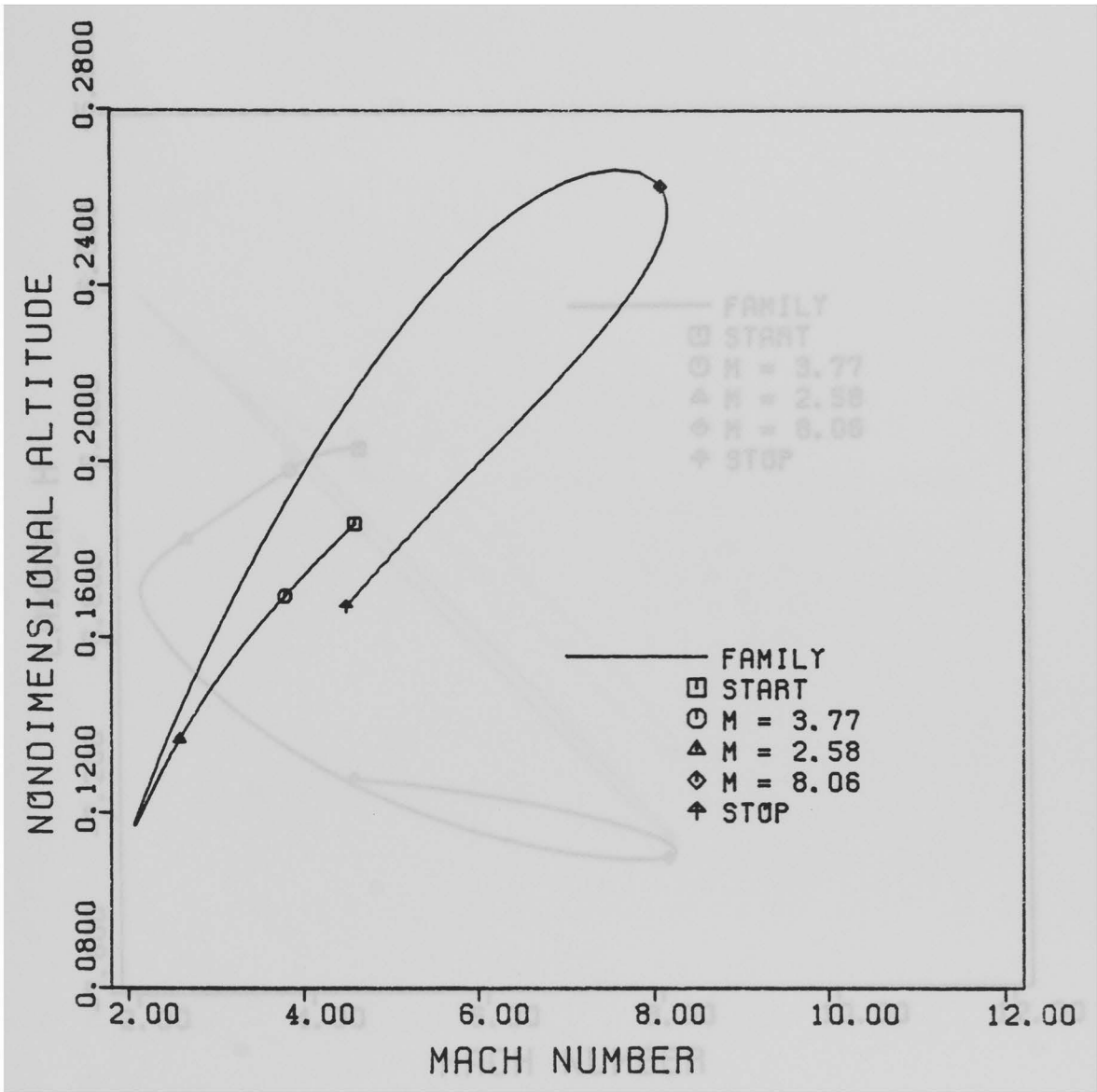

Figure 7a Periodic Family, Spherical Earth.

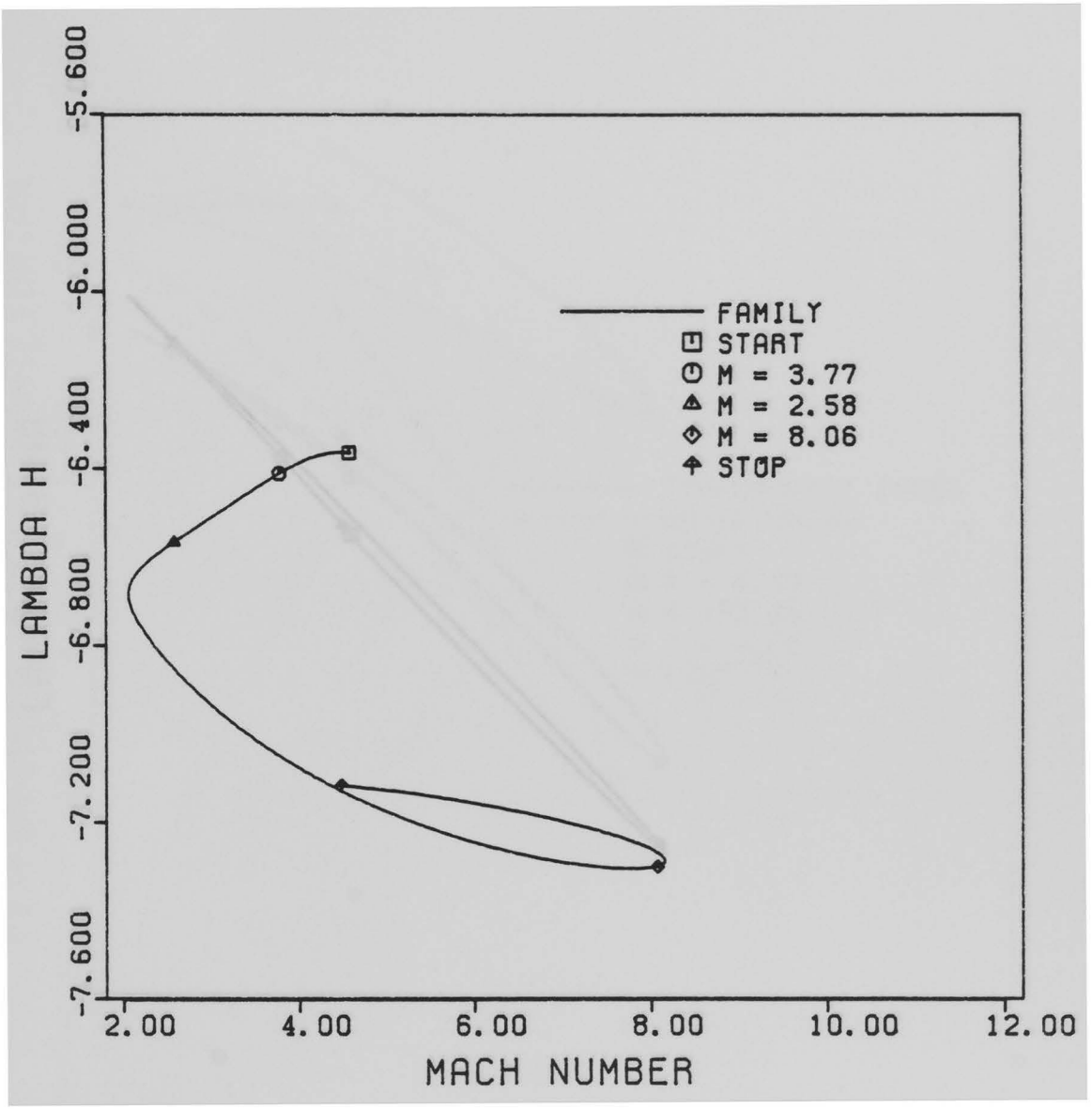

Figure 7b Periodic Family, Spherical Earth.

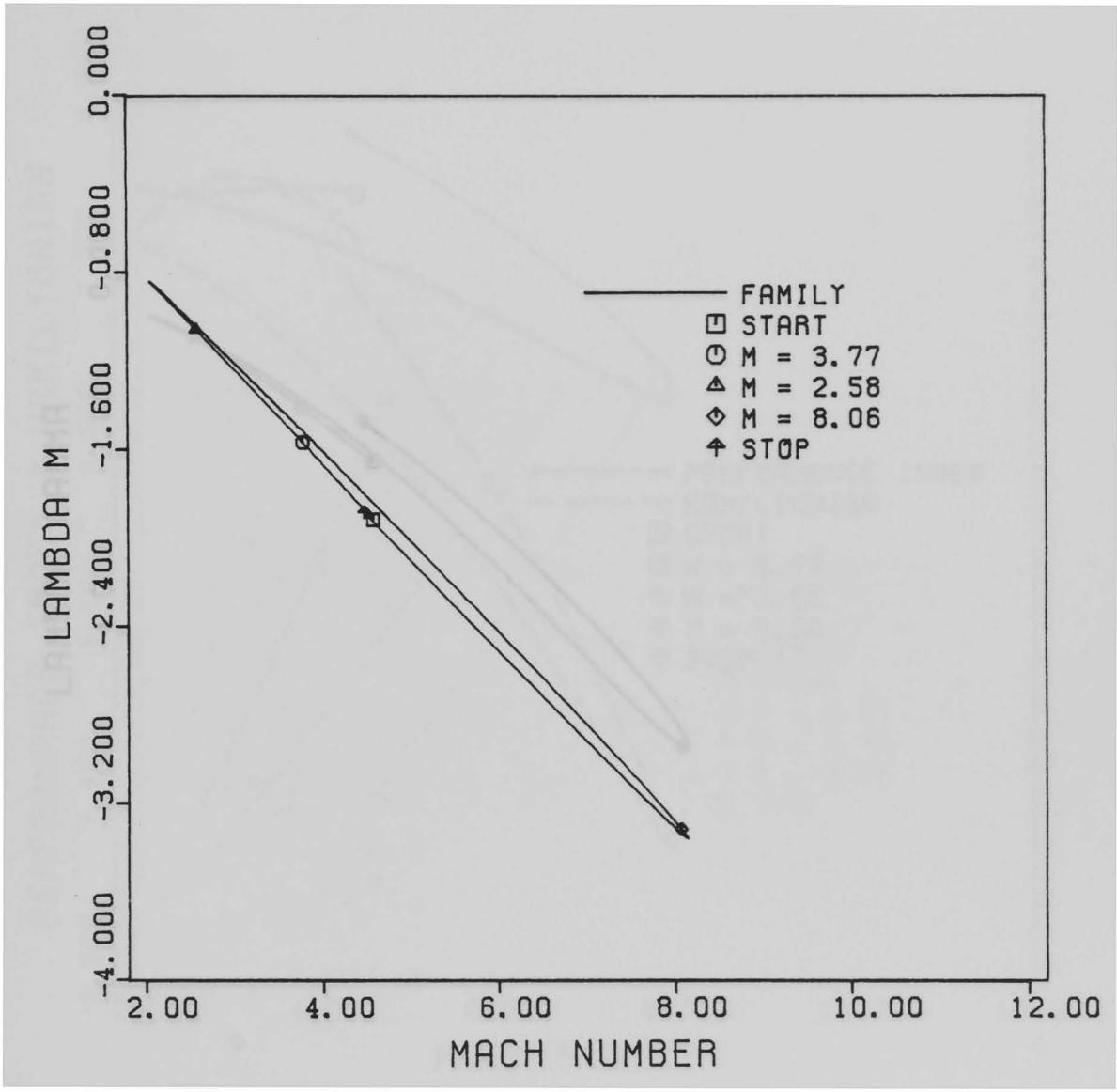

Figure 7c Periodic Family, Spherical Earth.

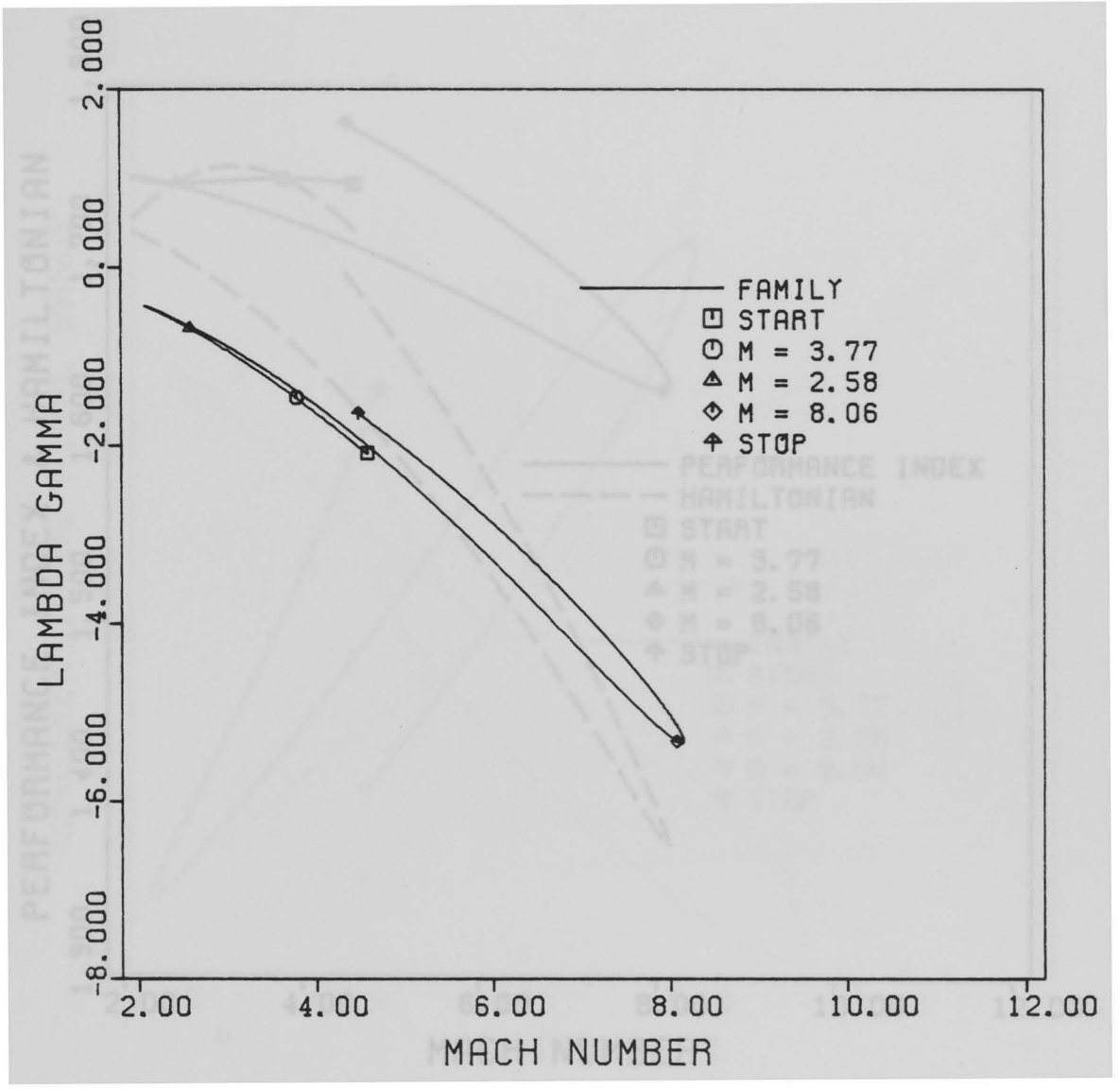

Figure 7d Periodic Family, Spherical Earth.

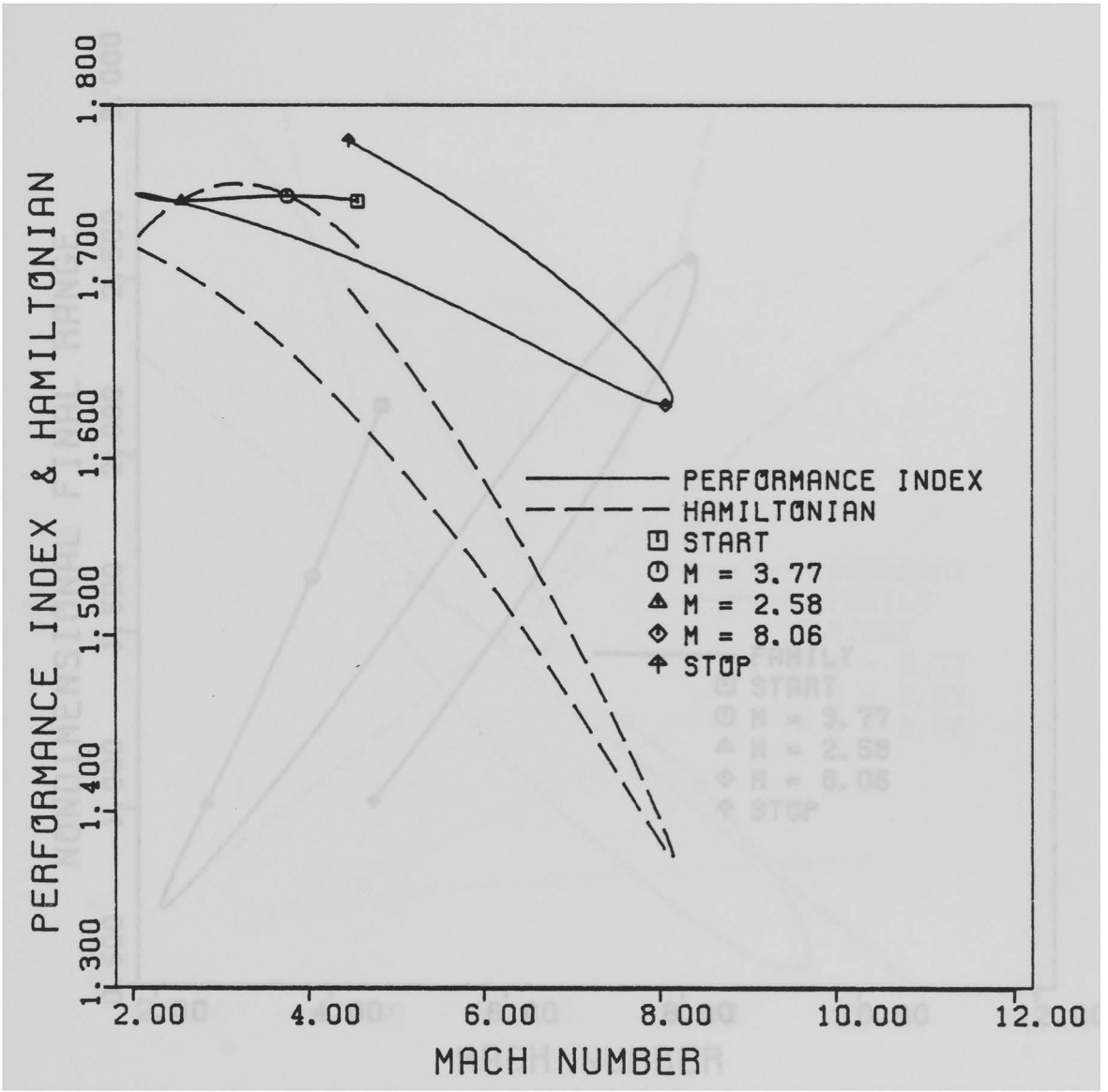

Figure 7e Periodic Family, Spherical Earth.

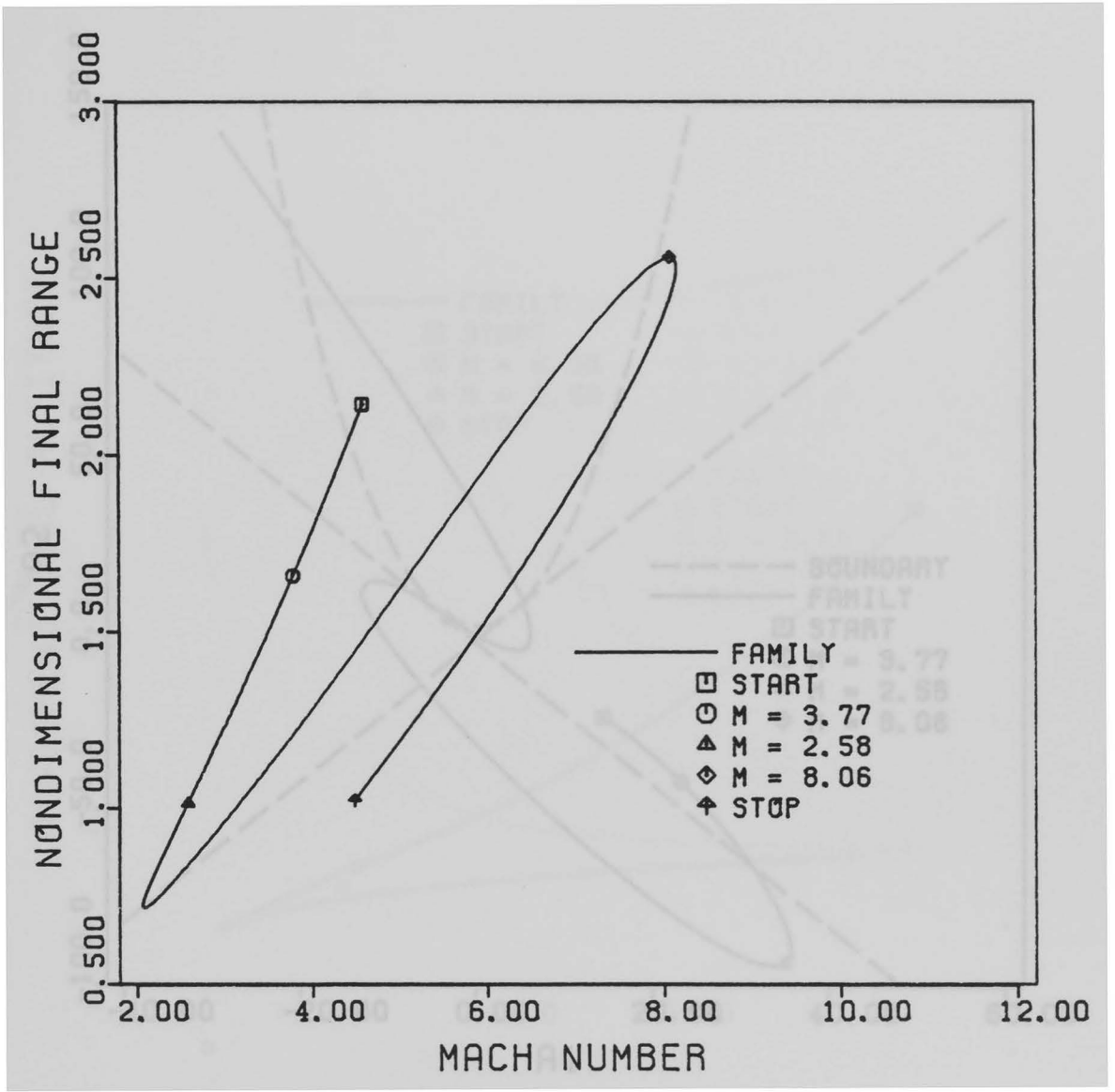

Figure 7f Periodic Family, Spherical Earth.

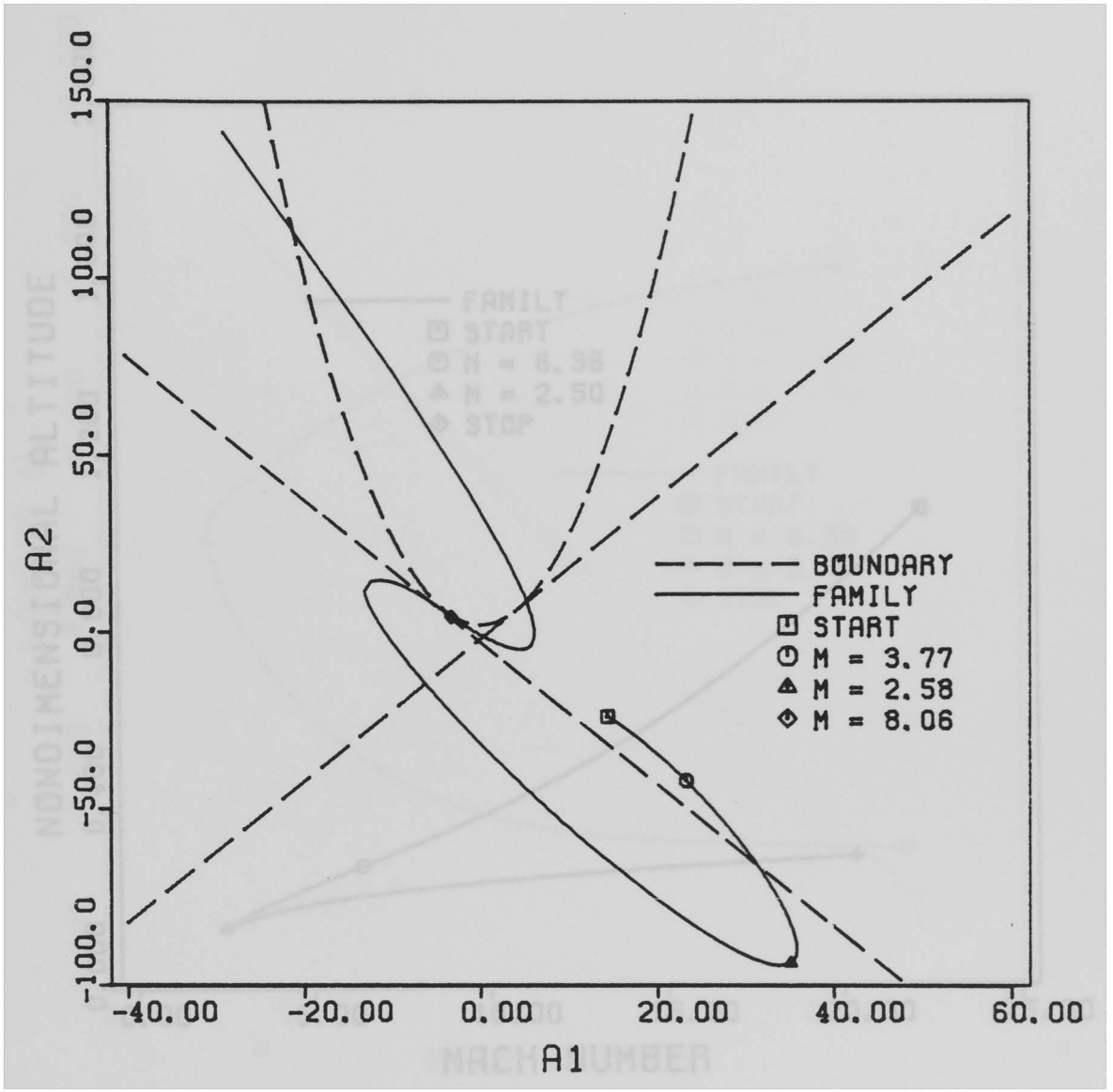

Figure 7g Periodic Family, Spherical Earth.

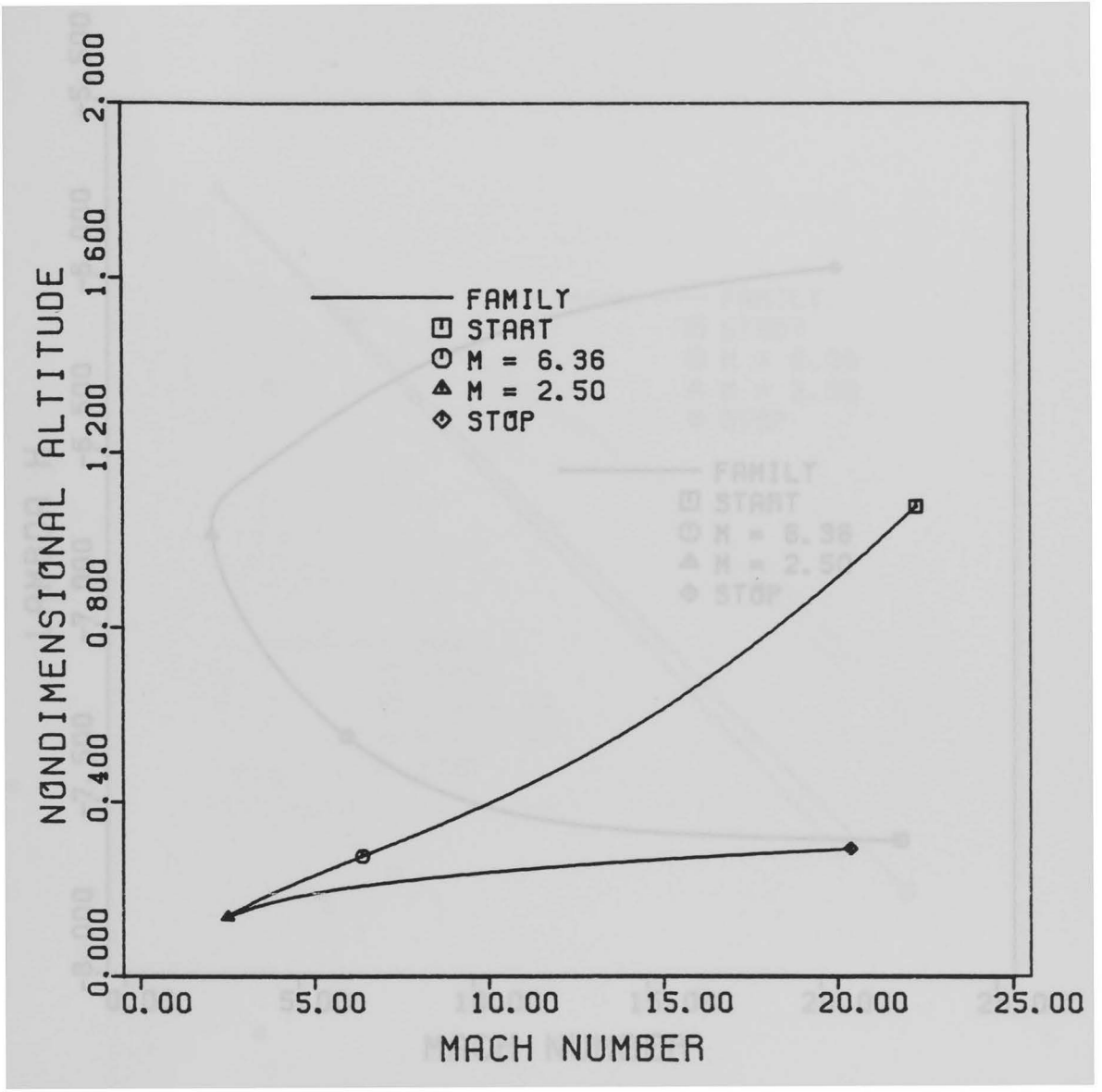

Figure 8a Periodic Family, Flat Earth.

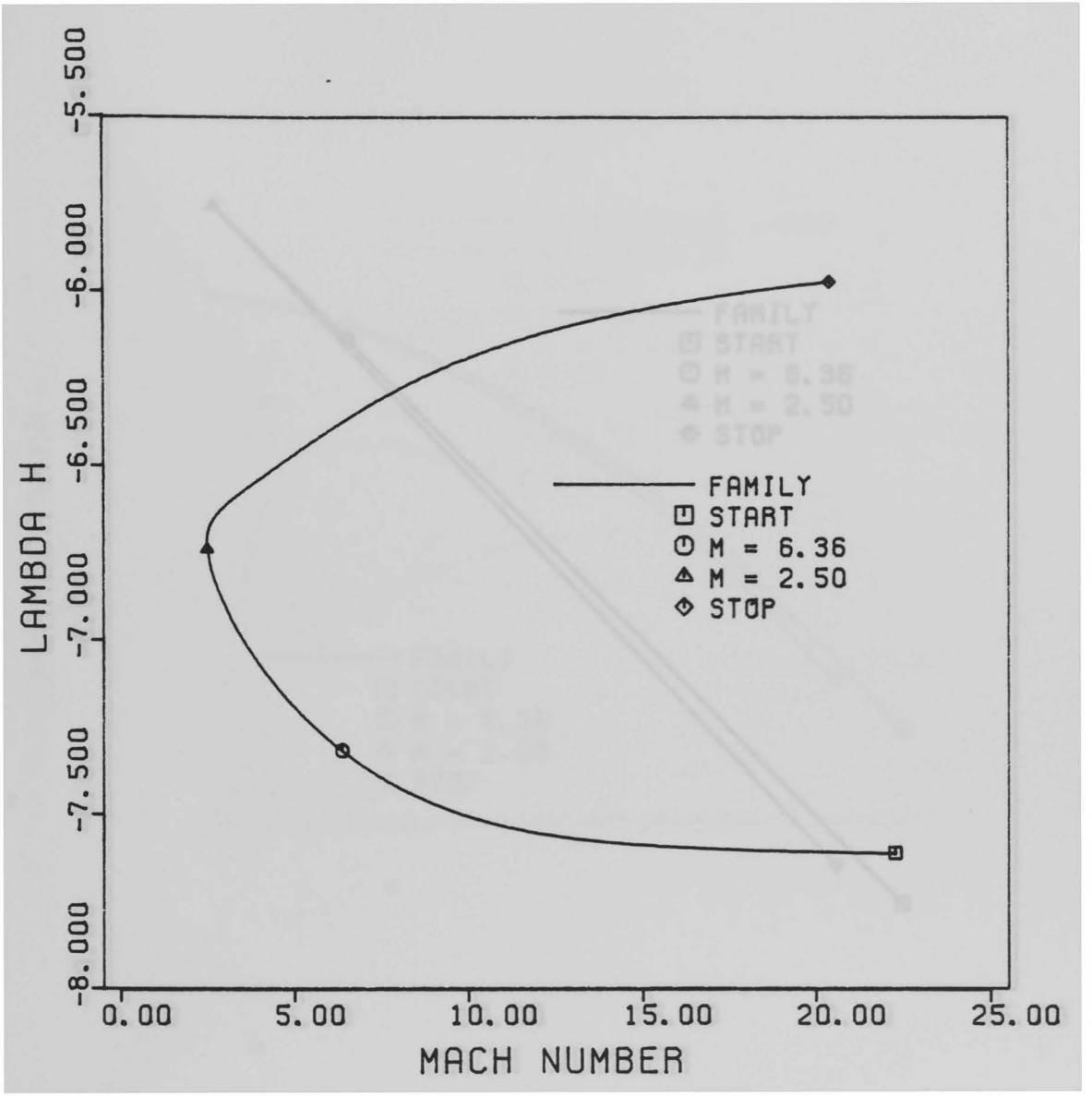

Figure 8b Periodic Family, Flat Earth.

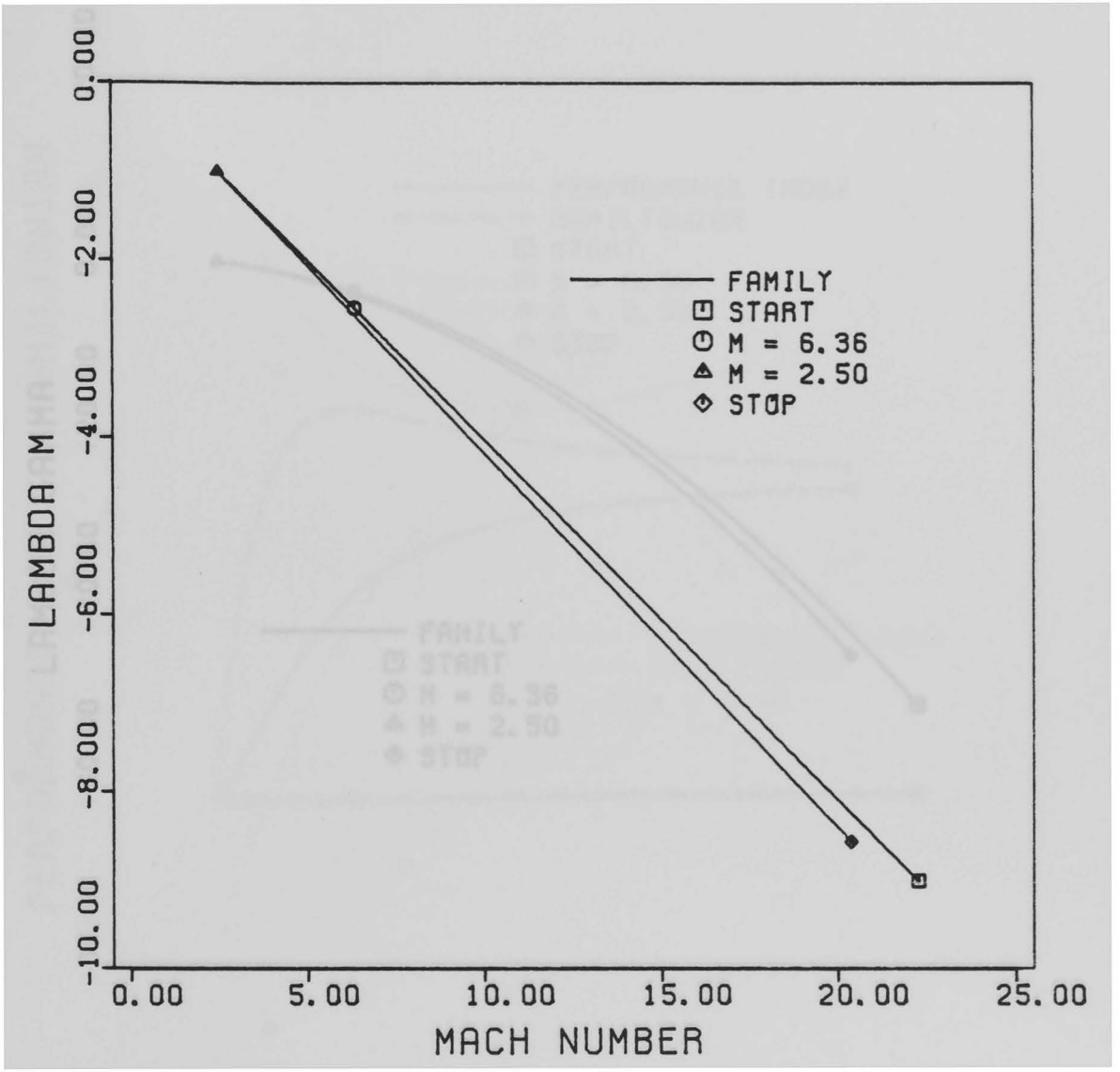

Figure 8c Periodic Family, Flat Earth.

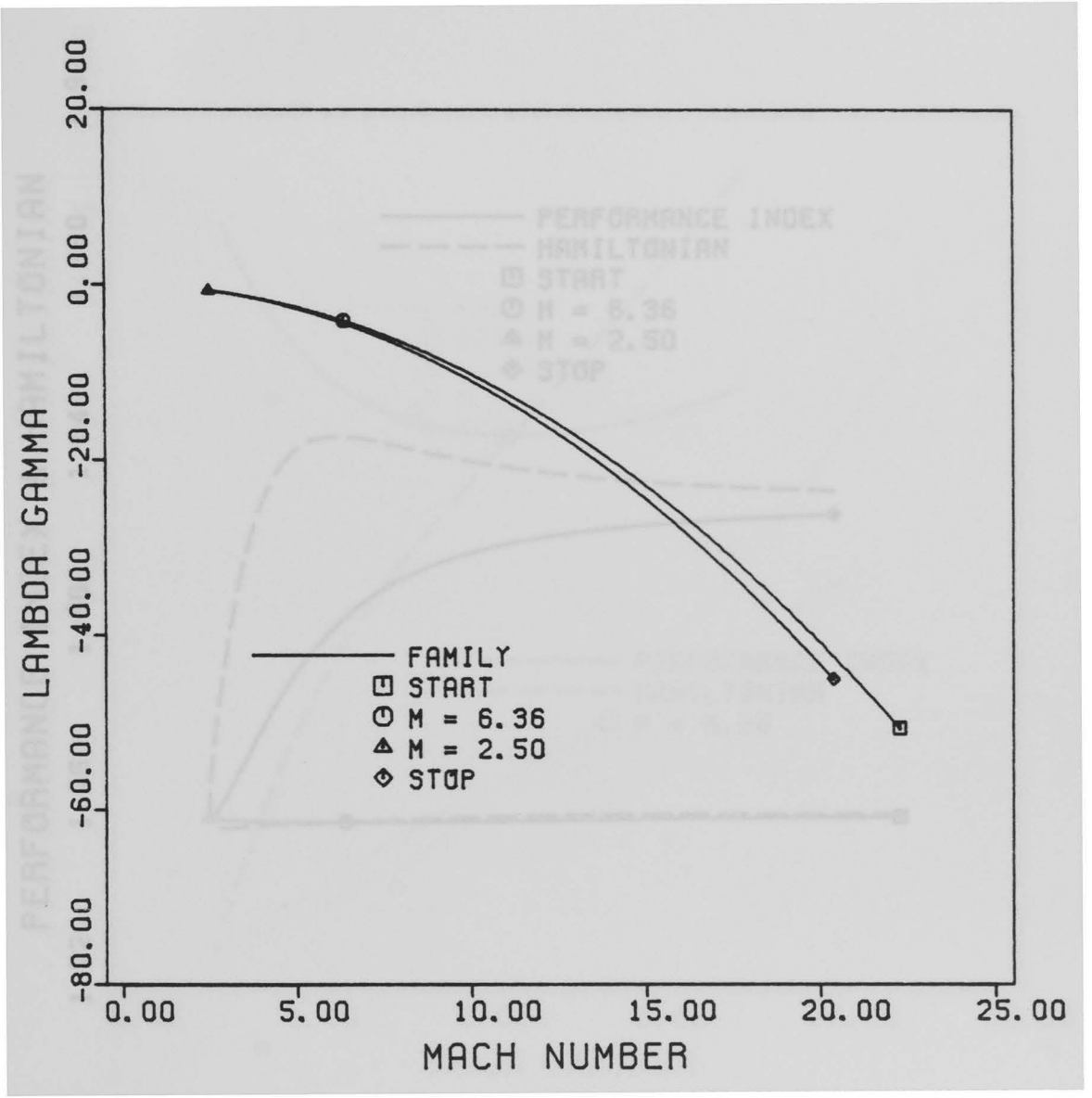

Figure 8d Periodic Family, Flat Earth.

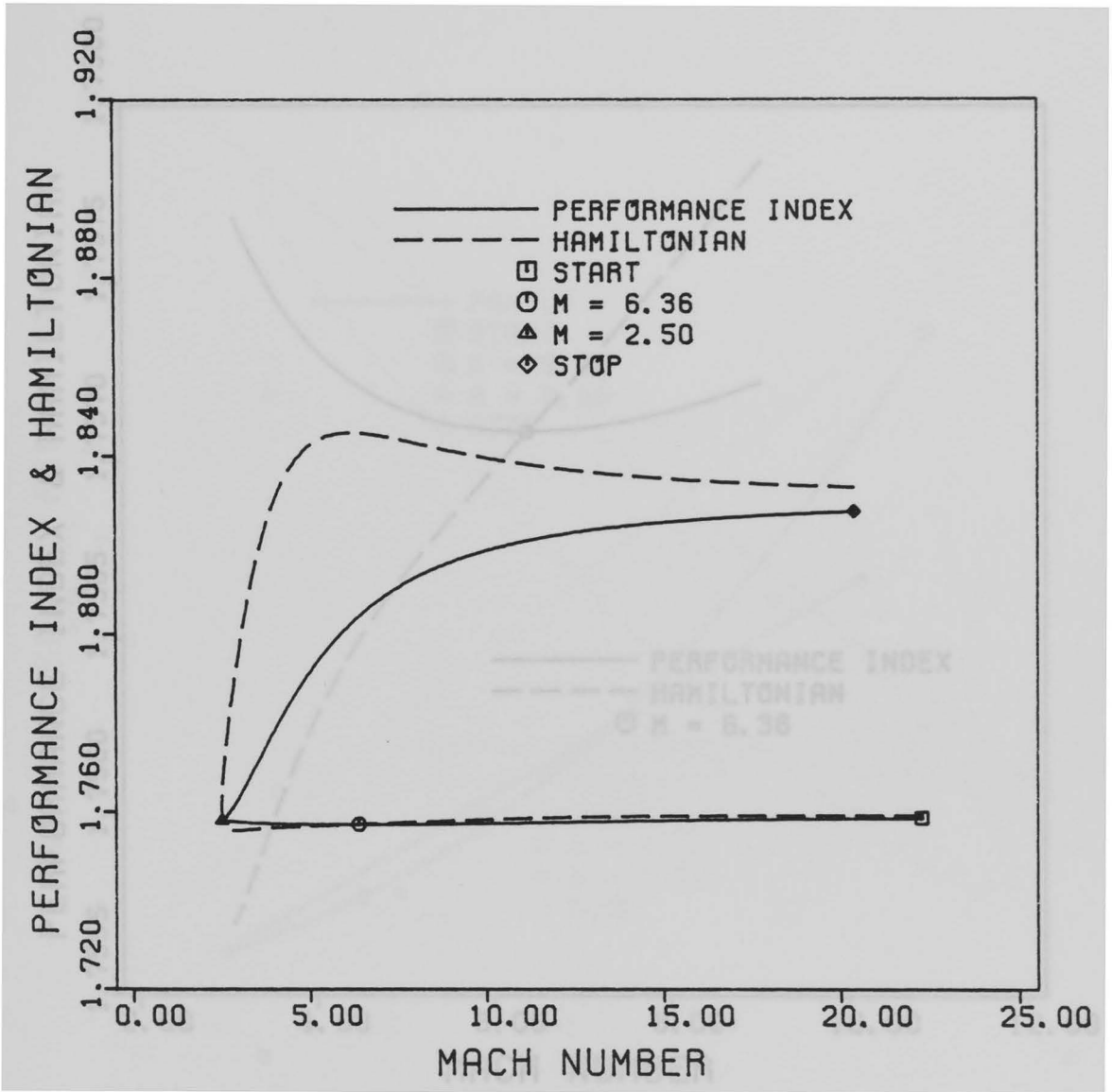

Figure 8e Periodic Family, Flat Earth.

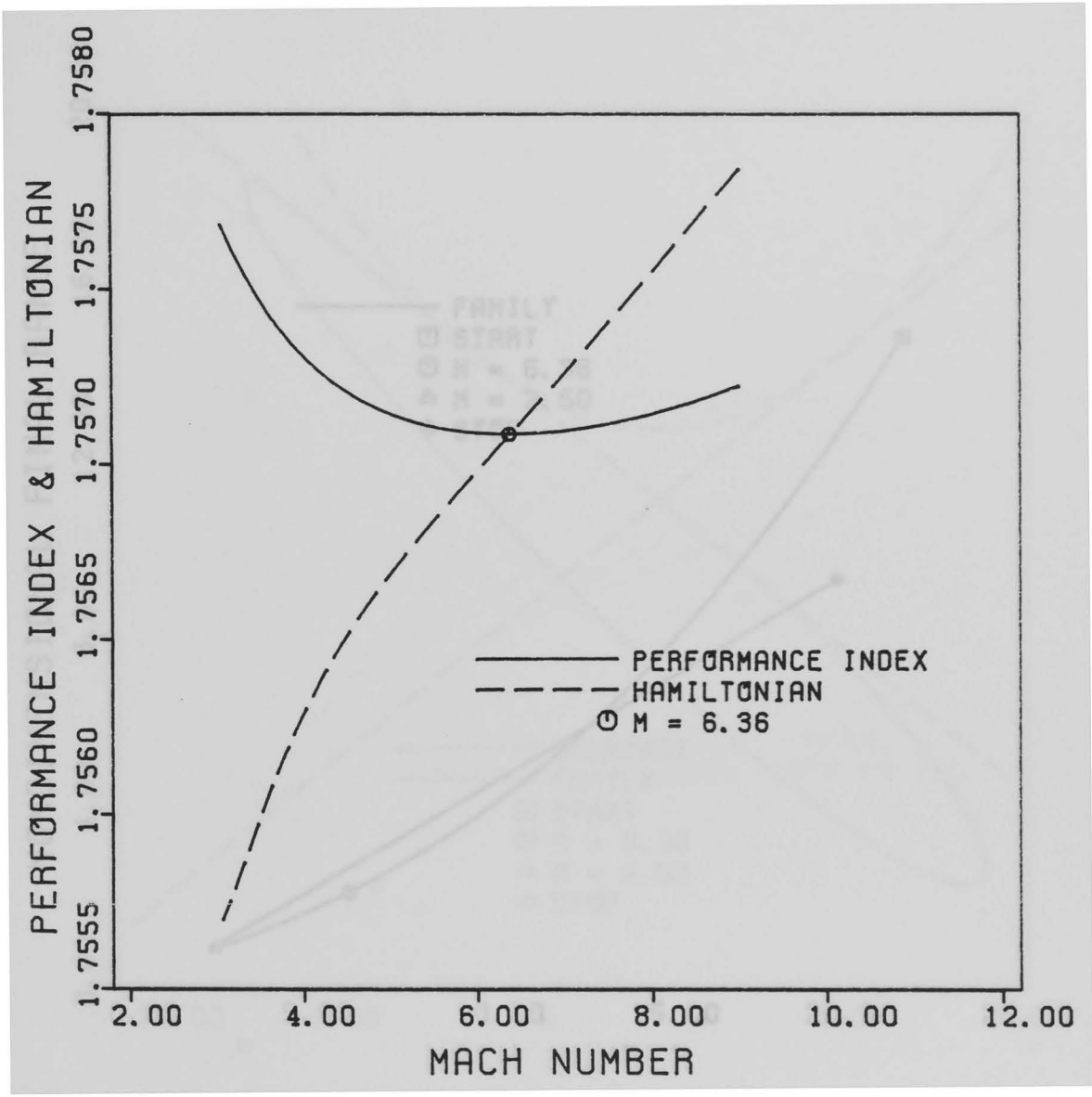

Figure 8f Periodic Family, Flat Earth.

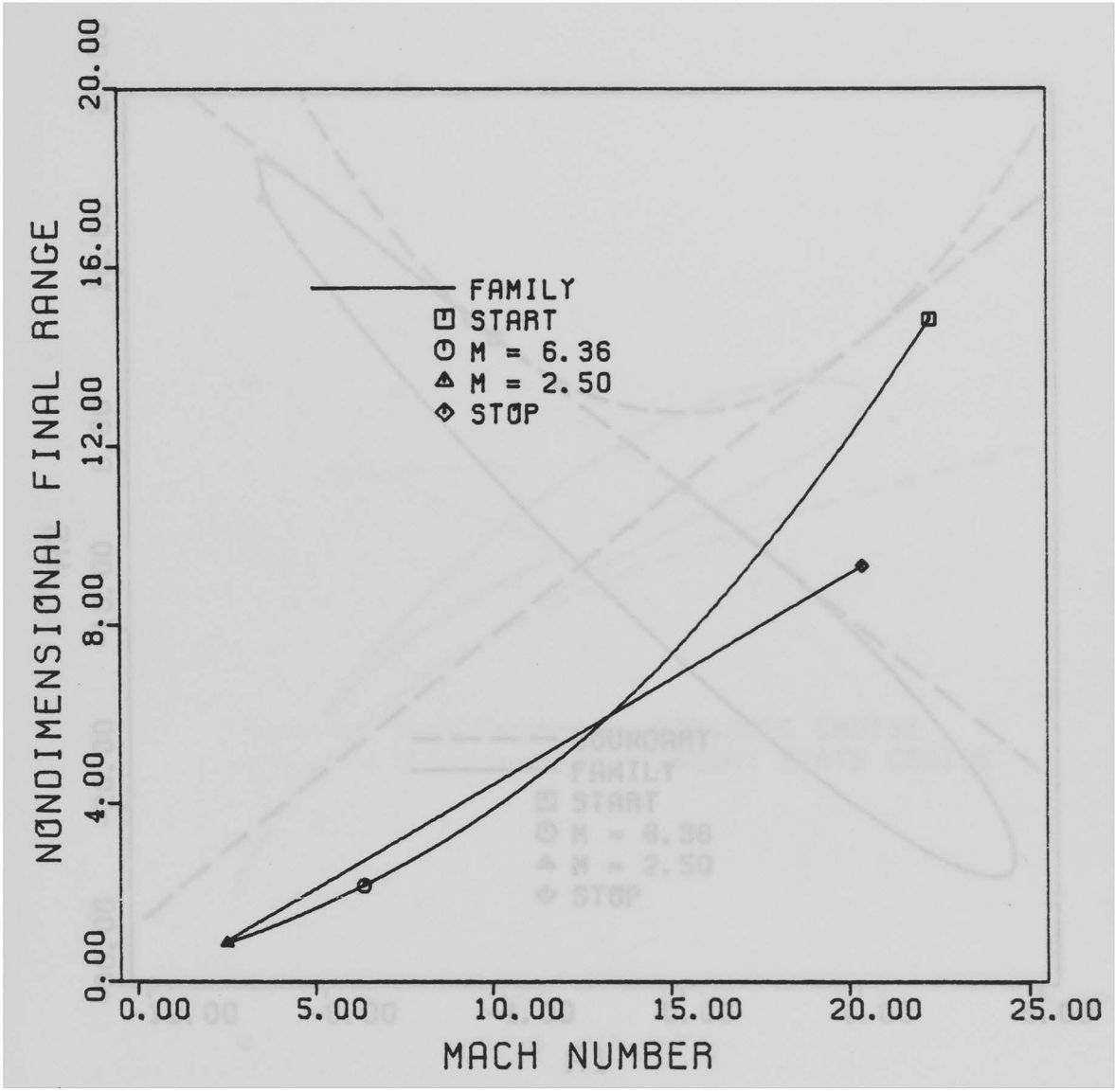

Figure 8g Periodic Family, Flat Earth.

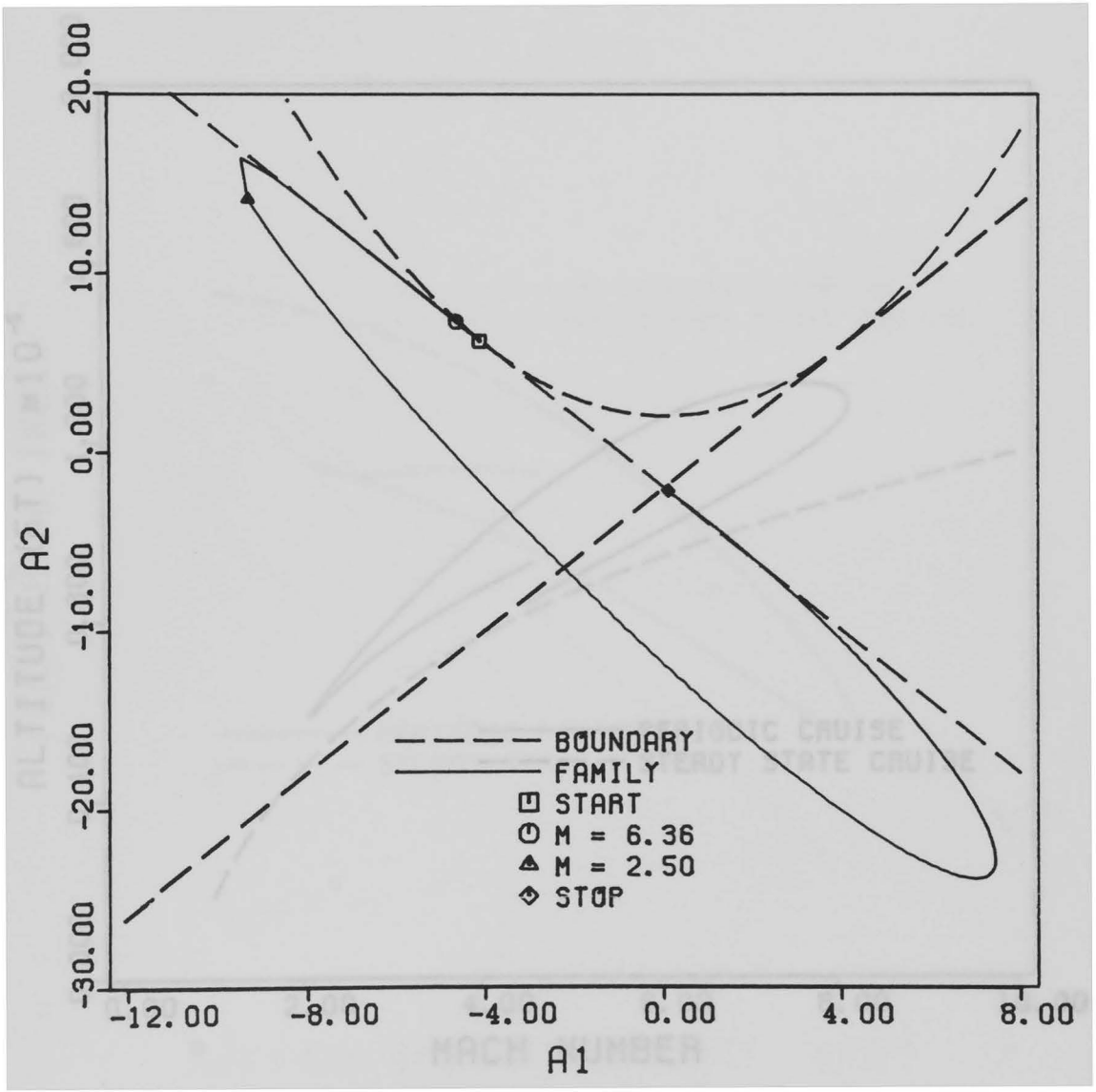

Figure 8h Periodic Family, Flat Earth.

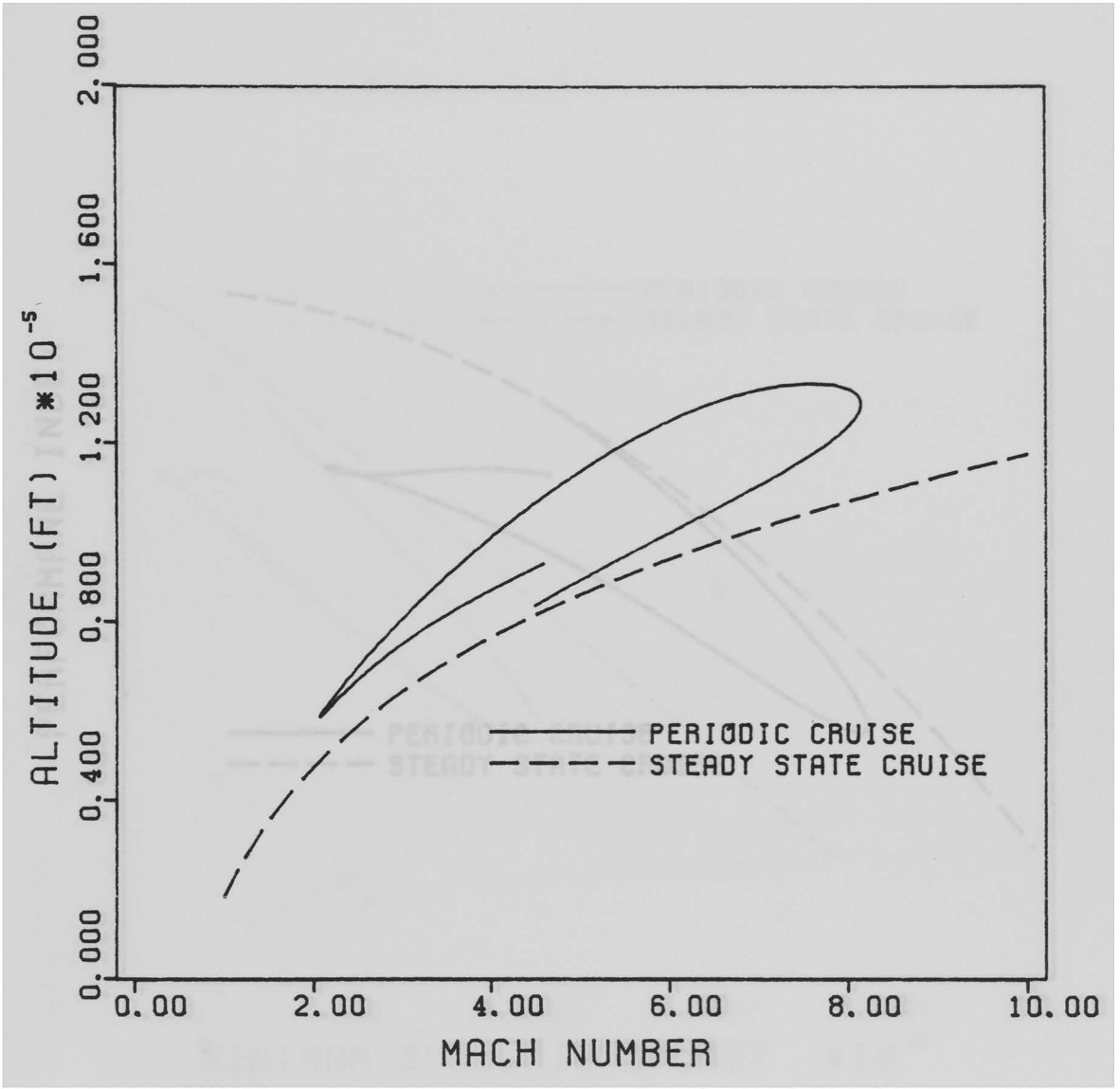

Figure 9a Periodic vs. Steady State, Spherical Earth.

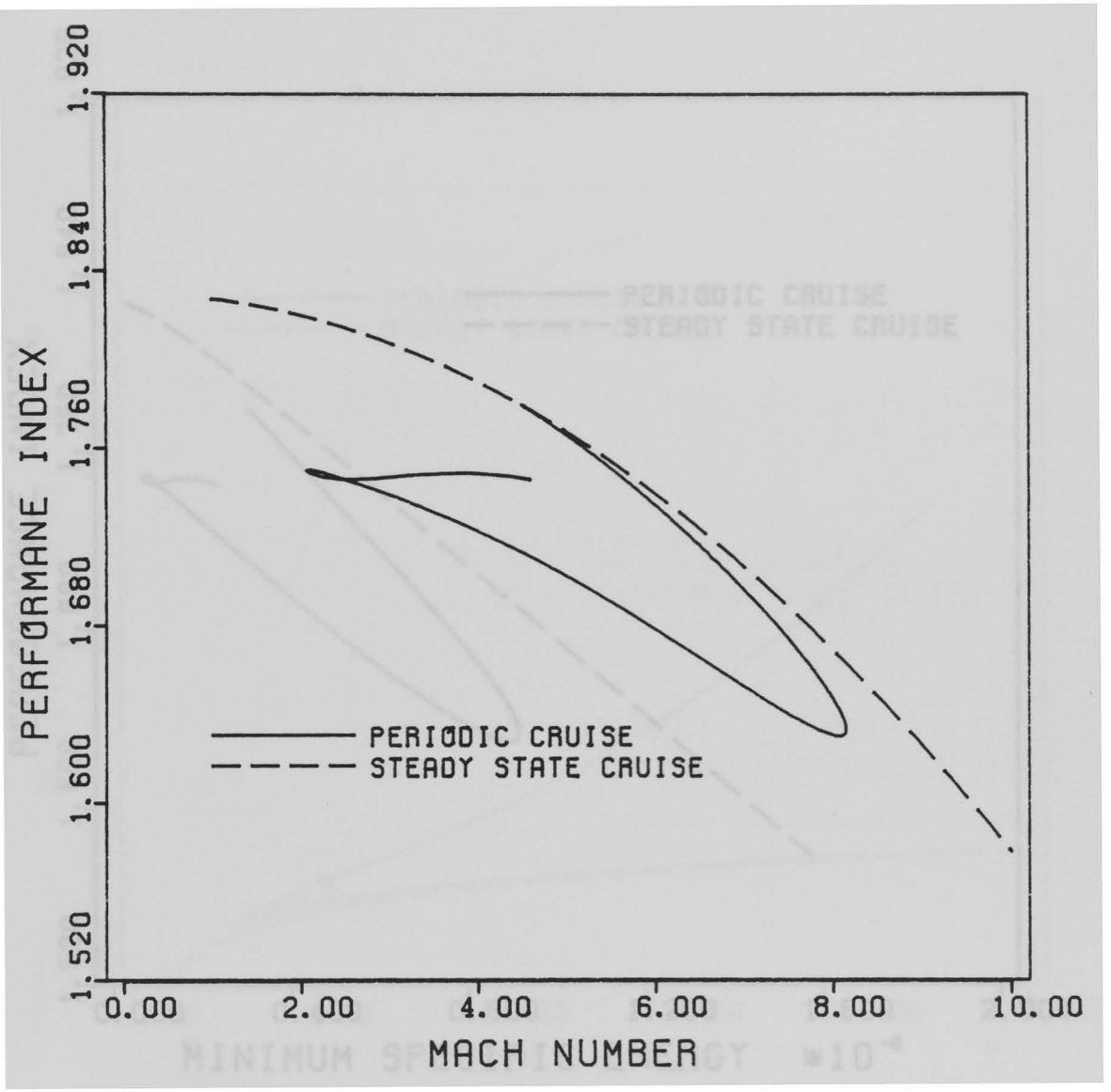

Figure 9b Periodic vs. Steady State, Spherical Earth.

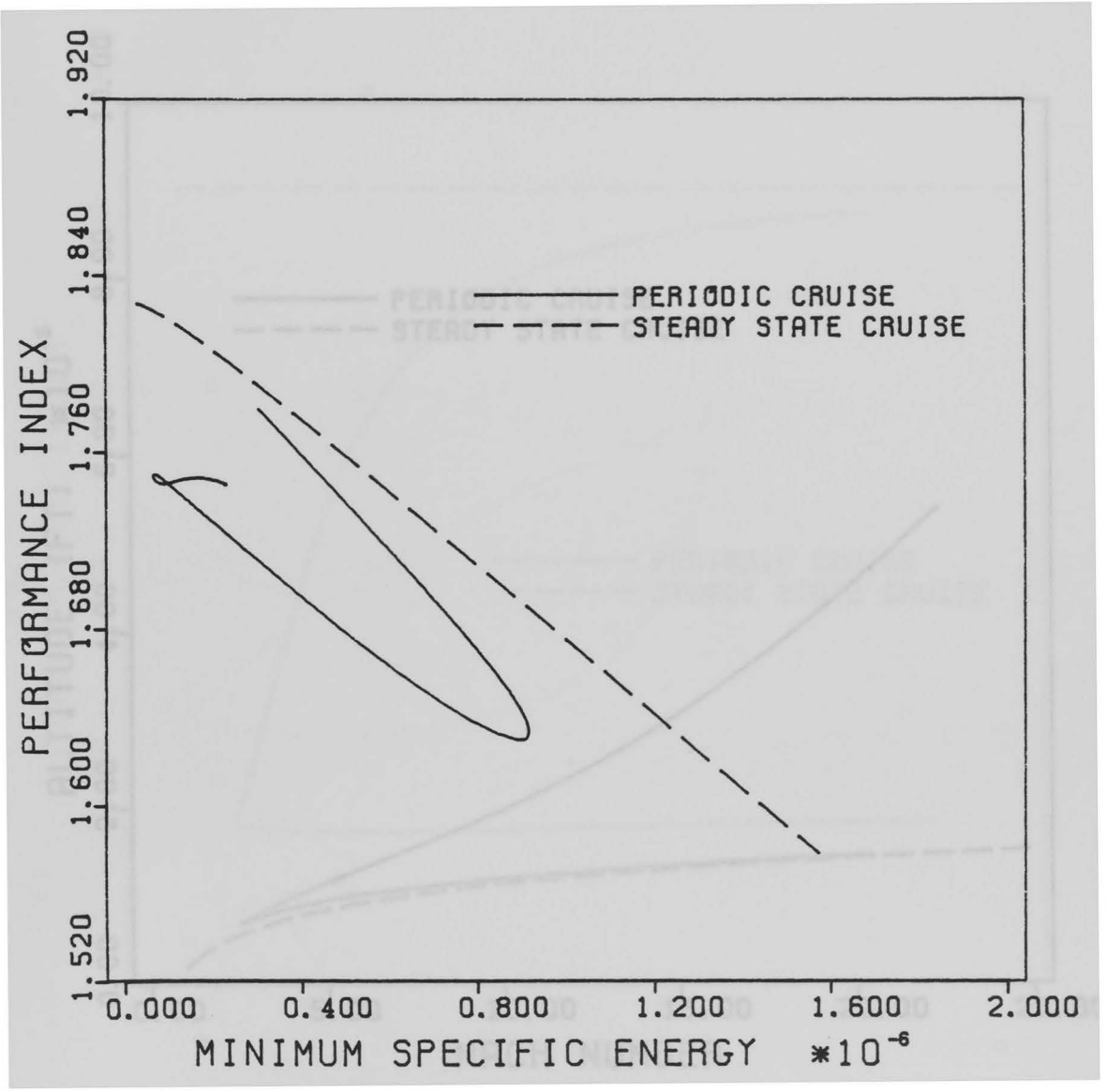

Figure 9c Periodic vs. Steady State, Spherical Earth.

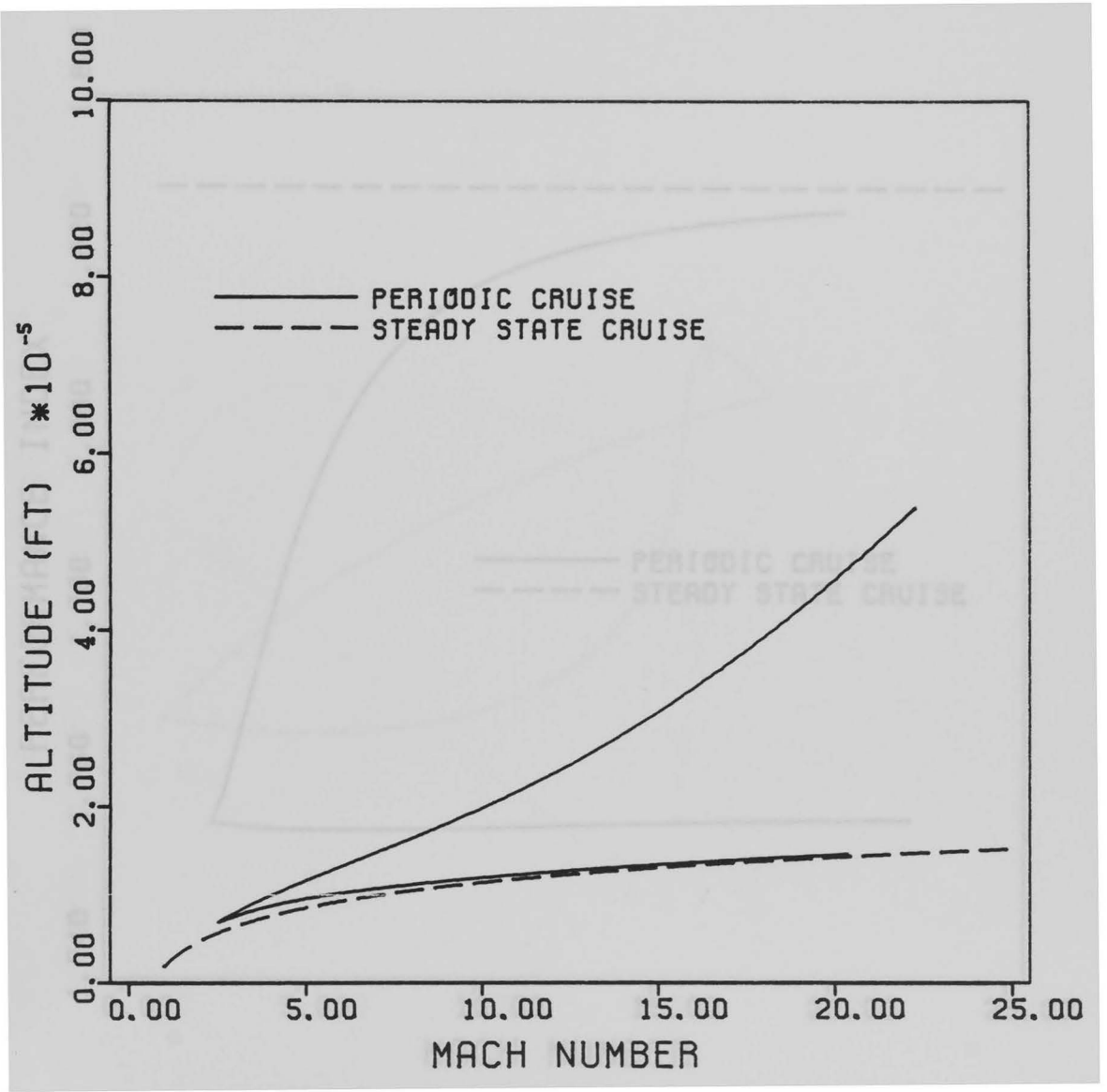

Figure 10a Periodic vs. Steady State, Flat Earth.

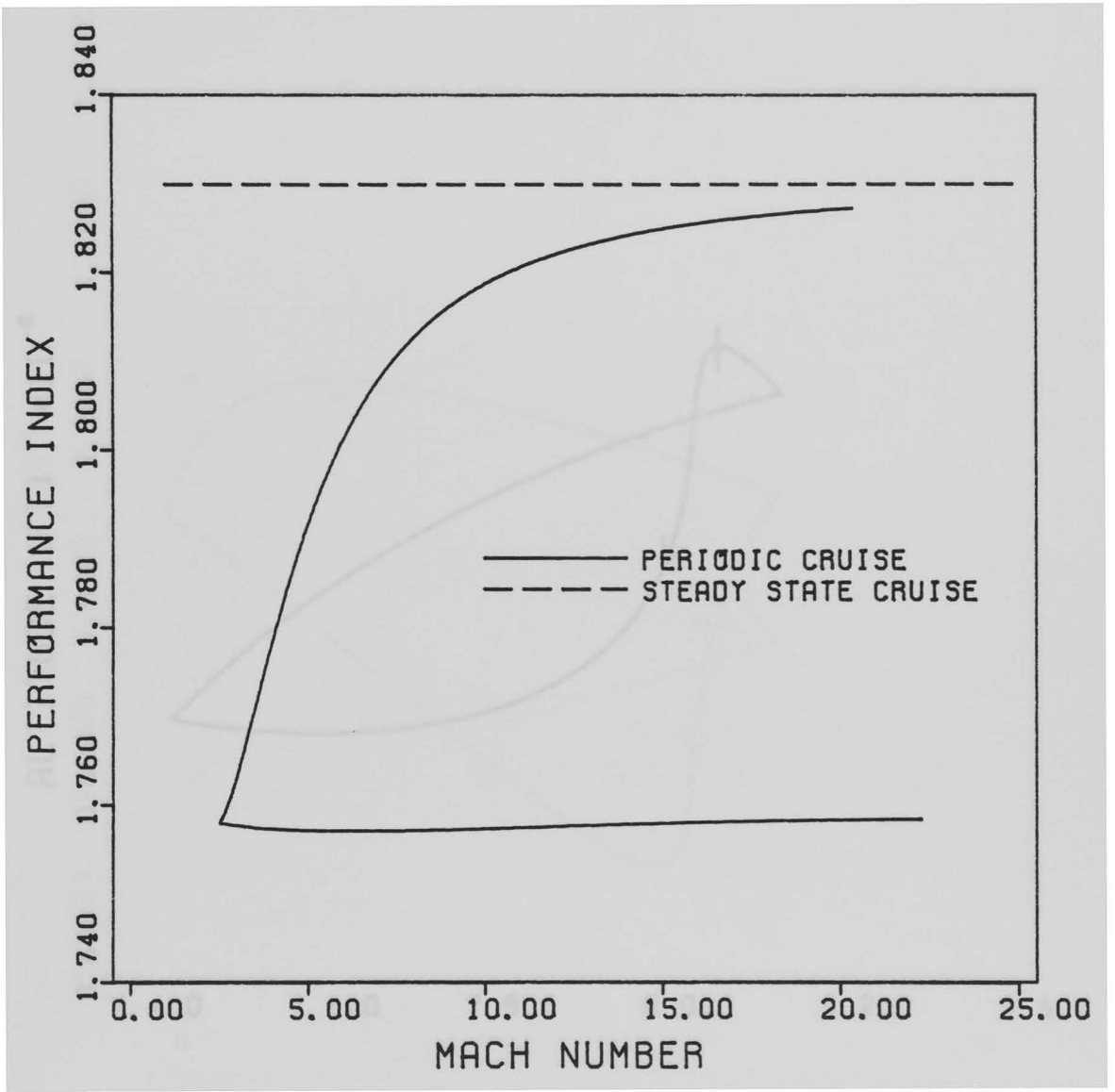

Figure 10b Periodic vs. Steady State, Flat Earth.

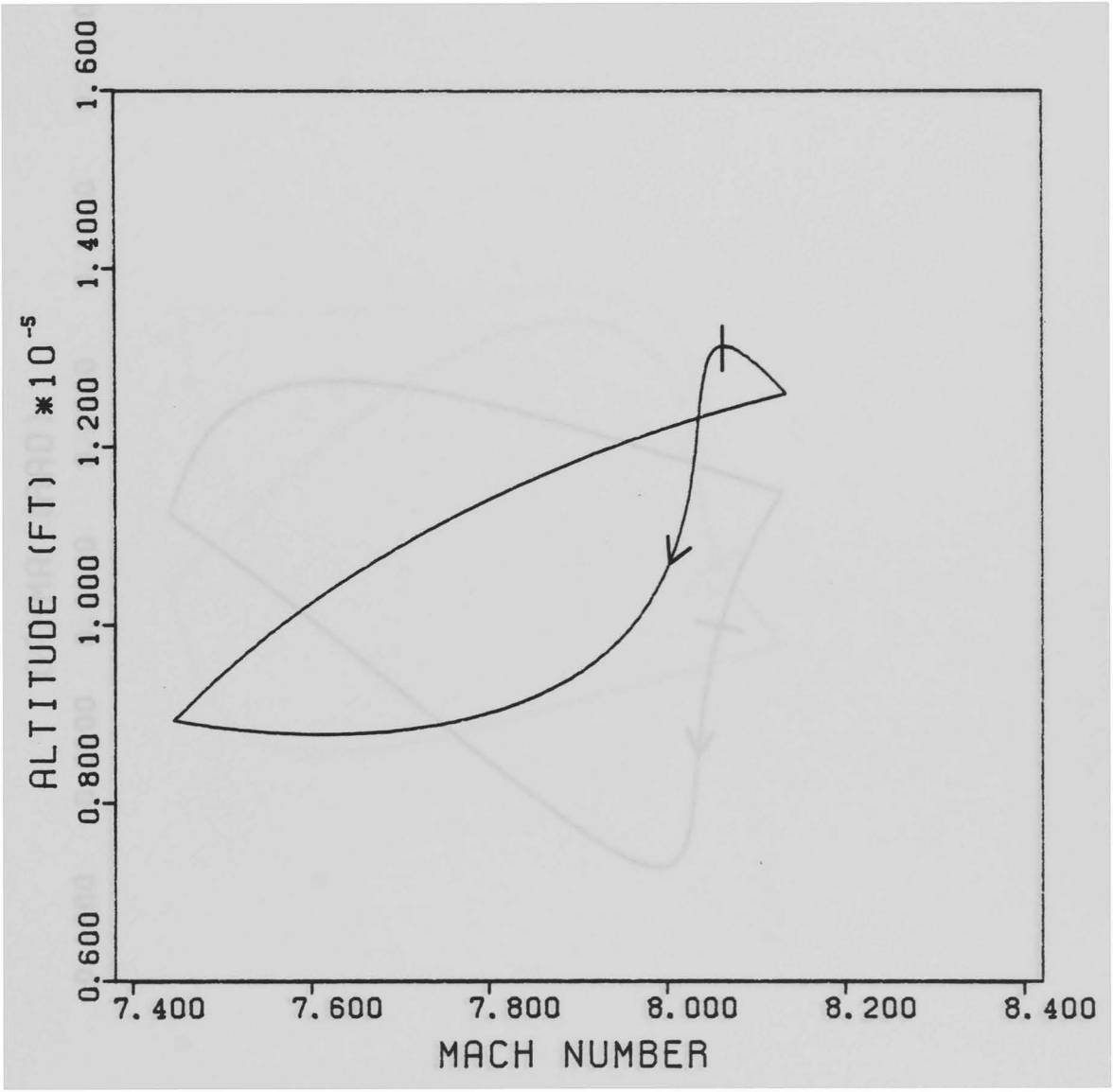

Figure 11a Phase Plane, M = 8.06 Cycle.

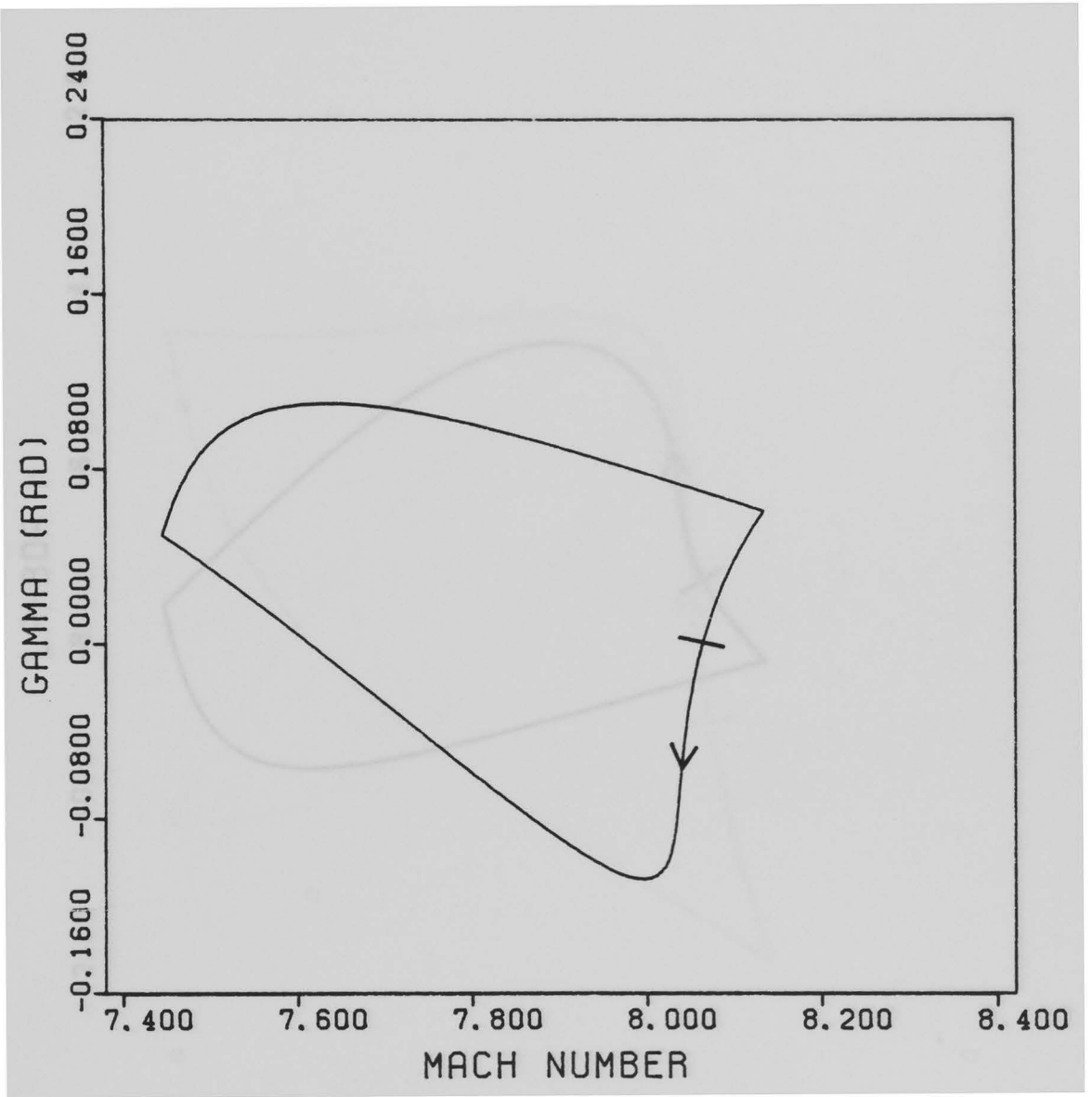

Figure 11b Phase Plane, M = 8.06 Cycle.

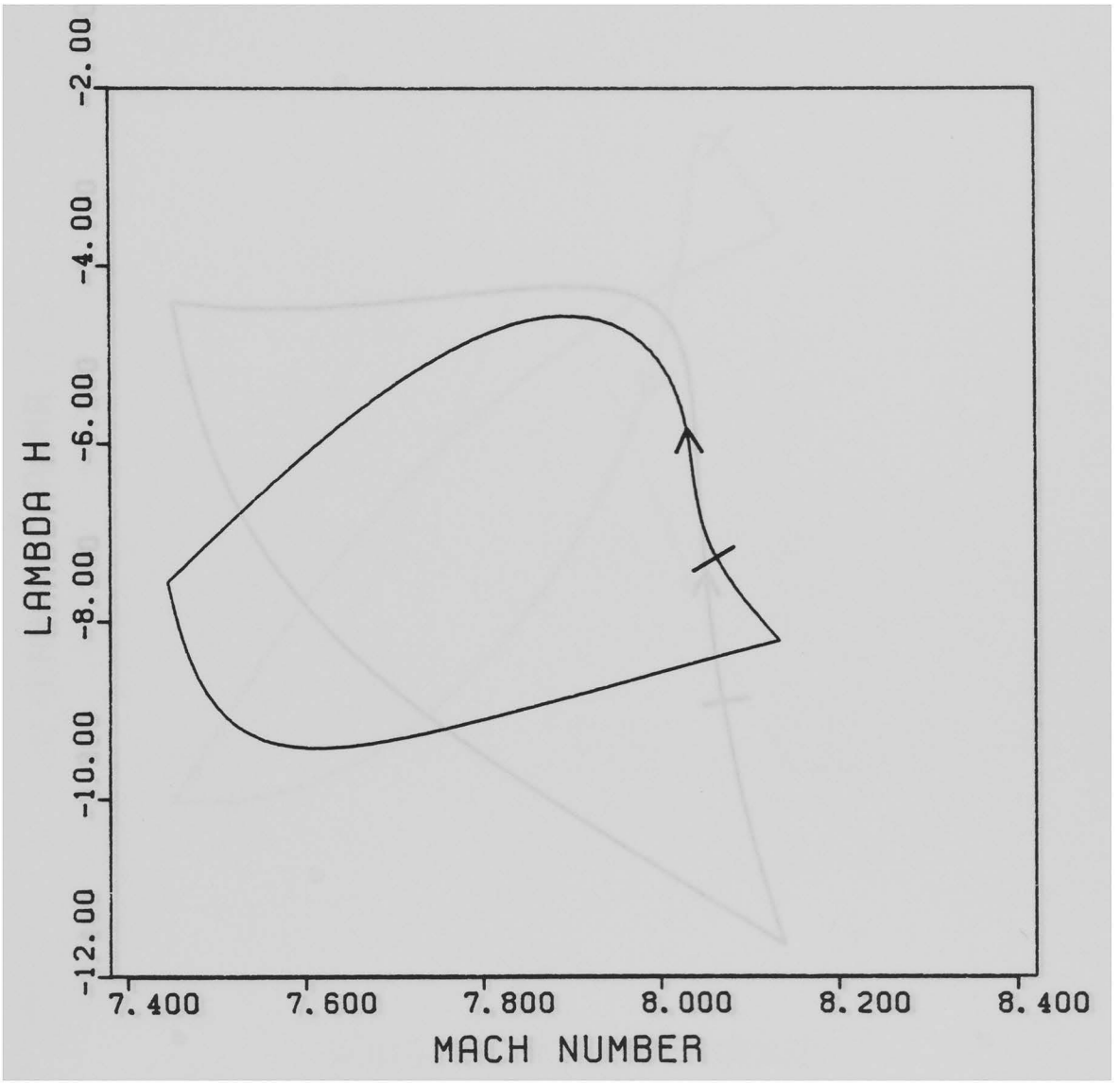

Figure 11c Phase Plane, M = 8.06 Cycle.

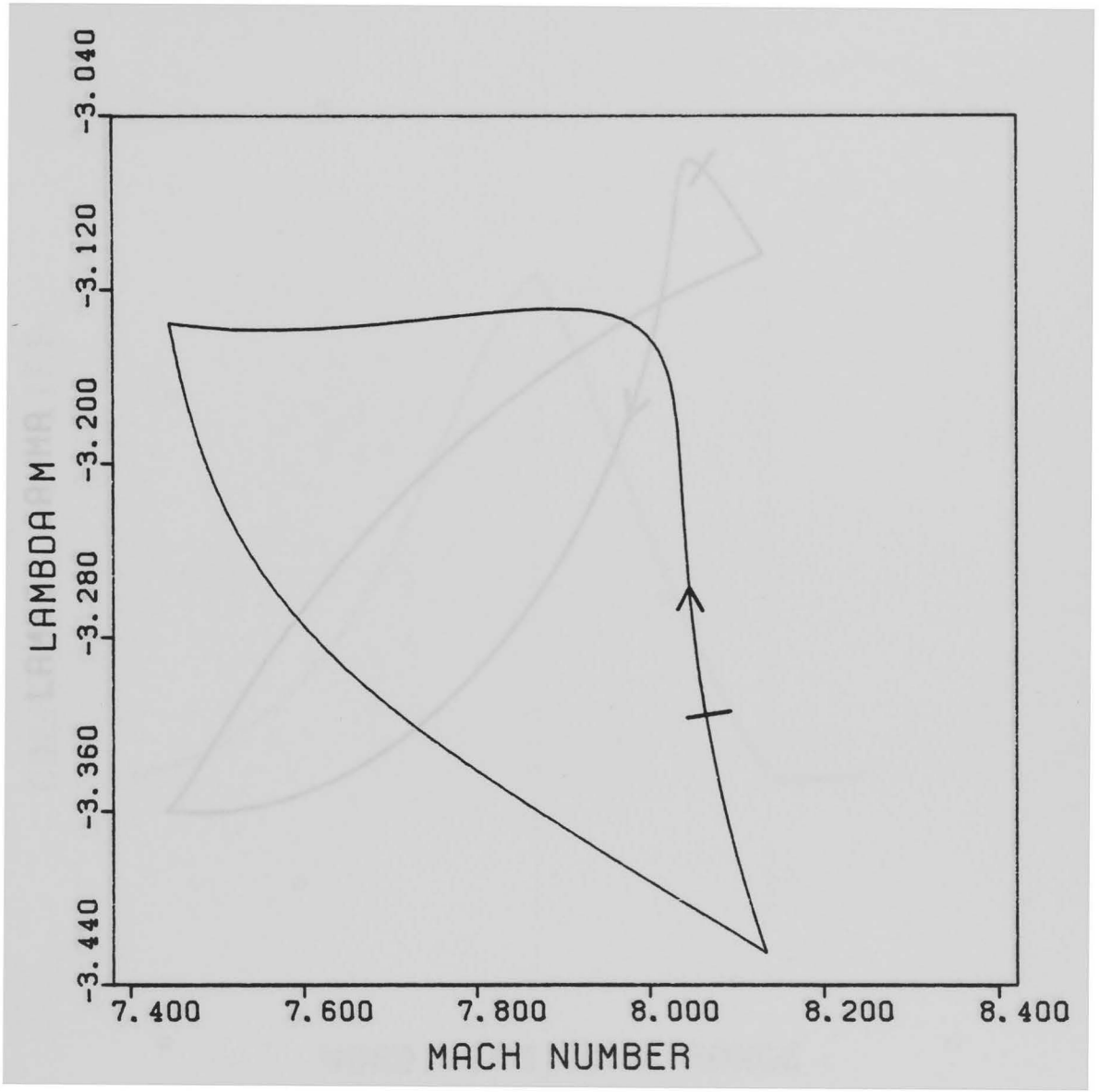

Figure 11d Phase Plane, M = 8.06 Cycle.

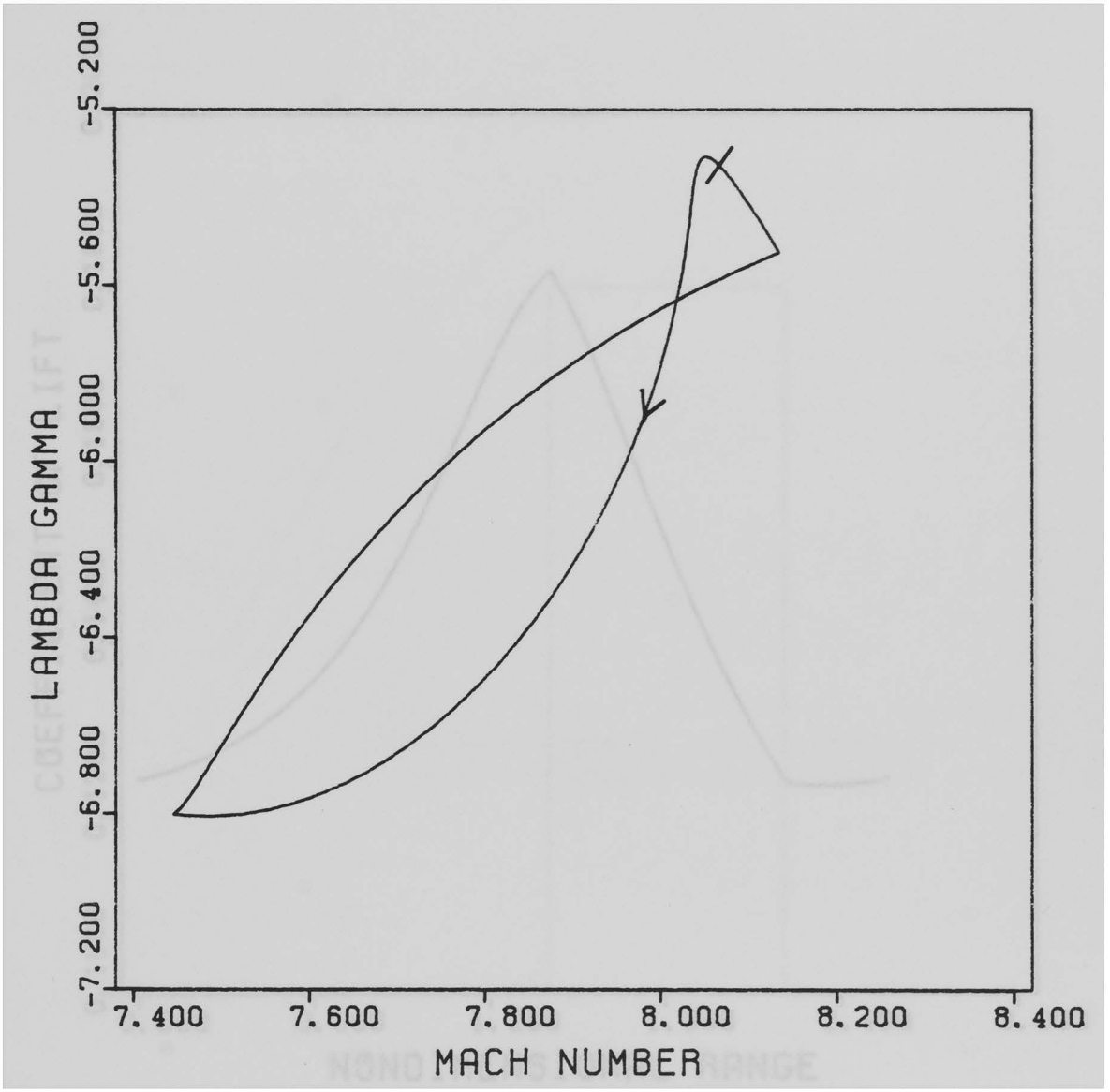

Figure 11e Phase Plane, M = 8.06 Cycle.

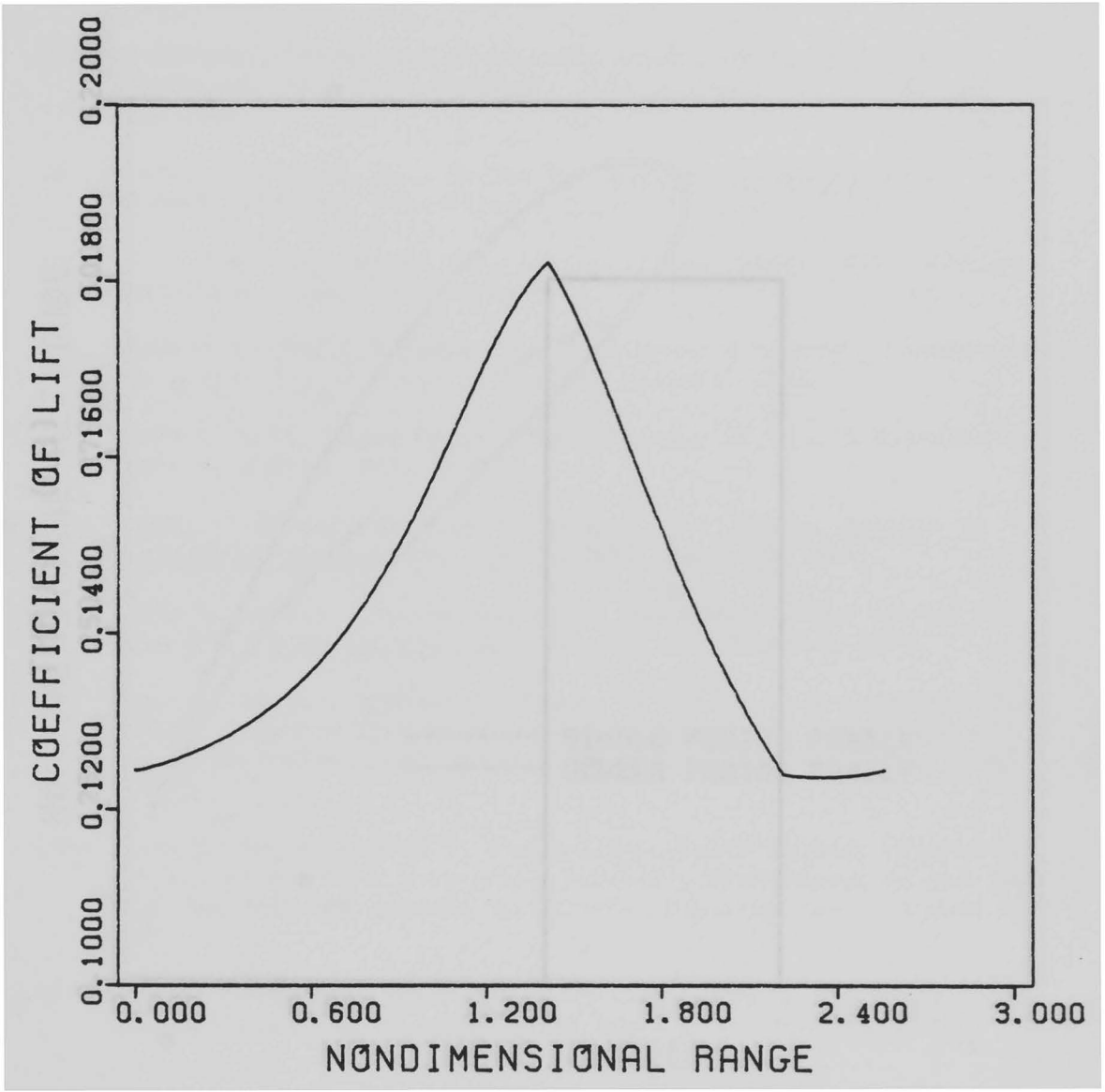

Figure 11f Control History, M = 8.06 Cycle.

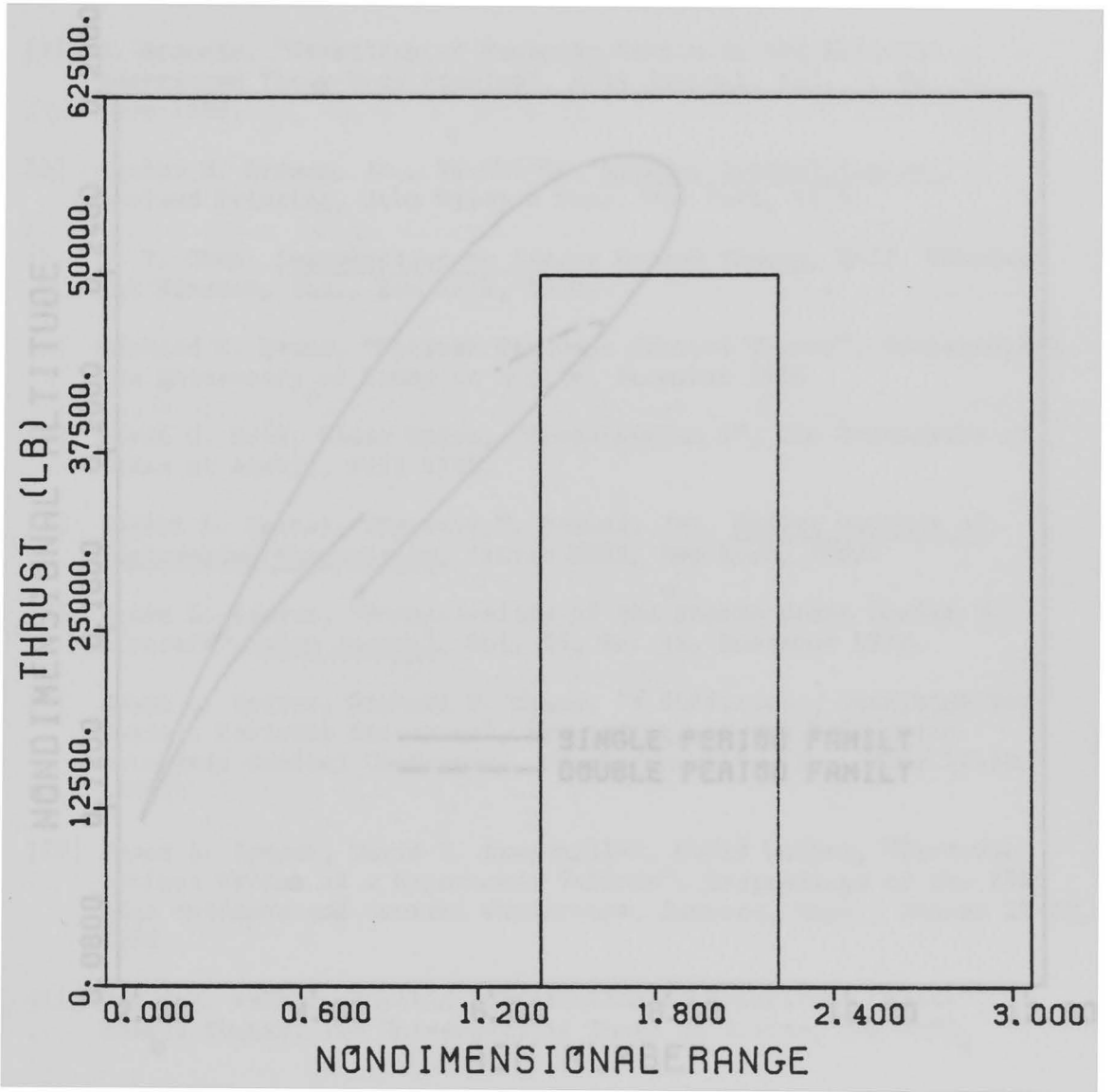

Figure 11g Control History, M = 8.06 Cycle.

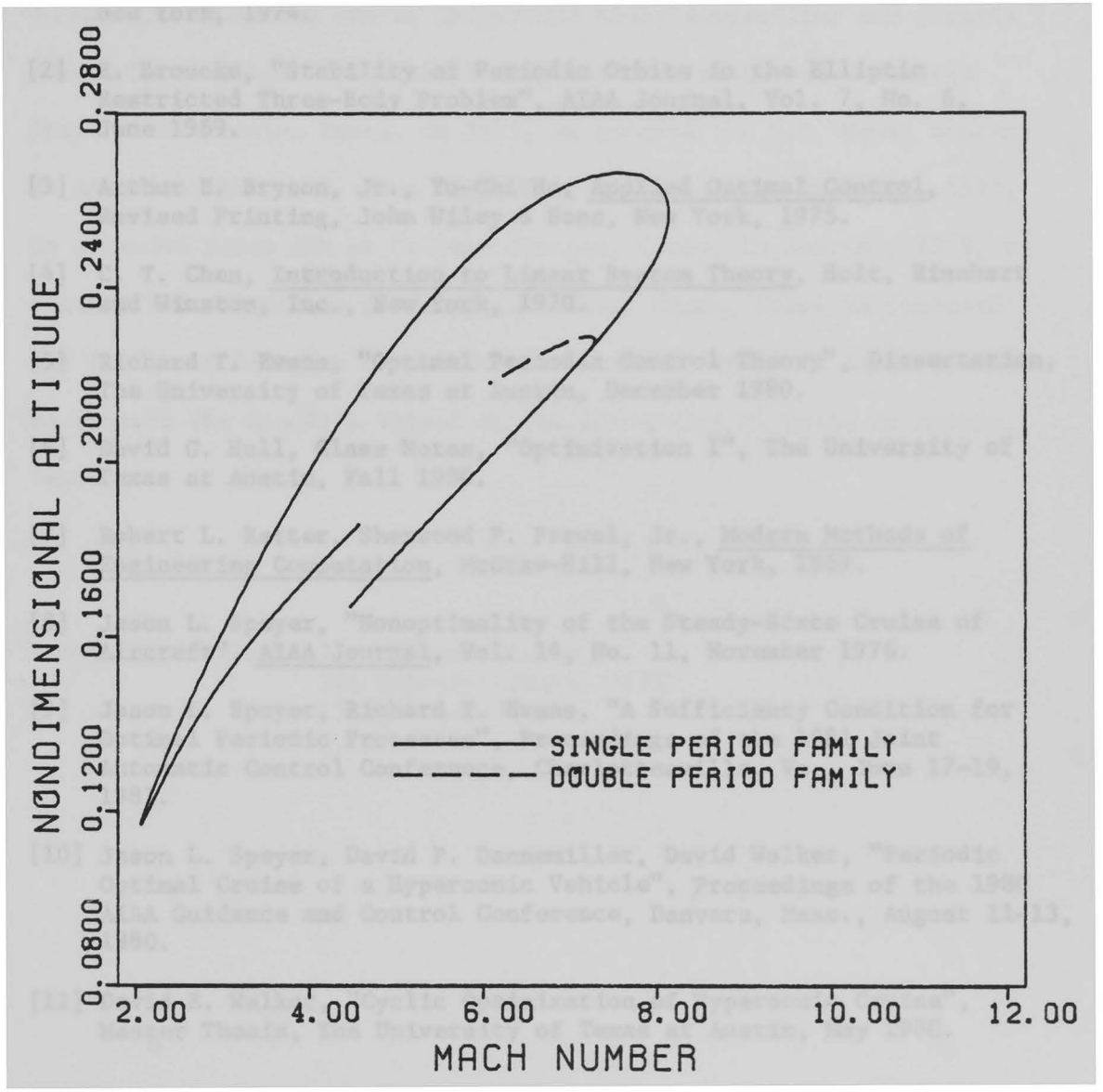

Figure 12 Bifurcation Point.

Bibliography

[1] William L. Brogan, Modern Control Theory, Quantum Publishers, Inc., New York, 1974.

[2] R. Broucke, "Stability of Periodic Orbits in the Elliptic Restricted Three-Body Problem", AIAA Journal, Vol. 7, No. 6, June 1969.

[3] Arthur E. Bryson, Jr., Yu-Chi Ho, Applied Optimal Control, Revised Printing, John Wiley & Sons, New York, 1975.

[4] C. T. Chen, Introduction to Linear System Theory, Holt, Rinehart and Winston, Inc., New York, 1970.

[5] Richard T. Evans, "Optimal Periodic Control Theory", Dissertation, The University of Texas at Austin, December 1980.

[6] David G. Hull, Class Notes, "Optimization I", The University of Texas at Austin, Fall 1980.

[7] Robert L. Ketter, Sherwood P. Prawel, Jr., Modern Methods of Engineering Computation, McGraw-Hill, New York, 1969.

[8] Jason L. Speyer, "Nonoptimality of the Steady-State Cruise of Aircraft", AIAA Journal, Vol. 14, No. 11, November 1976.

[9] Jason L. Speyer, Richard T. Evans, "A Sufficiency Condition for Optimal Periodic Processes", Proceedings of the 1981 Joint Automatic Control Conference, Charlottesville, Va., June 17-19, 1981.

[10] Jason L. Speyer, David P. Dannemiller, David Walker, "Periodic Optimal Cruise of a Hypersonic Vehicle", Proceedings of the 1980 AIAA Guidance and Control Conference, Danvers, Mass., August 11-13, 1980.

[11] David E. Walker, "Cyclic Optimization of Hypersonic Cruise", Master Thesis, The University of Texas at Austin, May 1980.

The vita has been removed from the digitized version of this document.